Noname manuscript No.
(will be inserted by the editor)

Numerical simulation of bed load and suspended load sediment transport using well-balanced numerical schemes

González-Aguirre, J. C. · González-Vázquez, J. A. · Alavez-Ramírez, J. · Silva, R. · Vázquez-Cendón, M. E.

Received: date / Accepted: date

Abstract Sediment transport can be modelled using hydrodynamic models based on shallow water equations coupled with the sediment concentration conservation equation and the bed conservation equation. The complete system of equations is made up of the energy balance law and the Exner equations. The numerical resolution for this complete system is done in a segregated manner. First, the hyperbolic part of the system of balance laws is resolved employing a finite volume scheme which is based on the Q-scheme of van Leer for computing the numerical flux also the numerical flux is computed by using an HLLCS approximate Riemann solver. As well, the hyperbolic system of balance laws is solve taken into account a non conservative form. The discretization of the source terms is carried out according to the numerical flux chosen. In the second stage, the bed conservation equation is resolved by using the approximation computed for the system of balance laws. The numerical schemes have been validate making comparison between the obtained numerical results and the experimental data for some ones physical experiments. The numerical results show in good agree with the experimental data.

División Acádemica de Ciencias Básicas, Universidad Juárez Autónoma de Tabasco
Carr. Cunduacán-Jalpa de Mendéz KM. 1, CP 86690, Cunduacán, Tabasco, México
E-mail: jcarlos.gonzalez@ujat.mx

Universidad Autónoma Metropolitana-Unidad Iztapalapa
Av. San Rafael Atlixco no.186 Ciudad de México, Mexico
E-mail: jgonzalezv@xanum.uam.mx

División Acádemica de Ciencias Básicas, Universidad Juárez Autónoma de Tabasco
Carr. Cunduacán-Jalpa de Mendéz KM. 1, CP 86690, Cunduacán, Tabasco, Mexico
E-mail: justino.alavez@ujat.mx

Instituto de Ingeniería, Universidad Nacional Autónoma de México
04510 Ciudad de México, Mexico
E-mail: rsilvac@iingen.unam.mx

Departamento de Matemática Aplicada, Universidade de Santiago de Compostela
15706 Santiago de Compostela, Spain
E-mail: elena.vazquez.cendon@usc.es

Keywords Sediment transport · Suspended load · Bedload · Finite volume method · Numerical simulation · Well-balanced schemes

1 Introduction

The mathematical modelling of sediment transport has become more important subject as of extreme hydrological events intensify and increase in numbers, as a result of climate change, see [8]. According to [23], the mathematical models proposed can be classified as fully coupled models (FCM), partially coupled models (PCM) and decoupled models (DM). The main difference between them is the manner in which they deal with the interaction between water flux, sediment transport and bed evolution. The FCM take into account the hydrodynamic and both the suspended load and the bedload transport. In these models, the bed evolution is modelled using the Exner equation (see [16, 17]) with source term. The PCM consider the hydrodynamic and suspended load sediment transport. In this kind of model, the bedload transport is not taken into account for modelling the bed evolution. The DM compute the sediment transport using the shallow water equations coupled with the bed conservation equation. In this kind of model the suspended load sediment transport is neglected.

Another difference between the models is the way as each one them consider the interaction between the flux, sediment transport and the morphological evolution inside the structure of mass conservation equation and momentum conservation equation. The FCM can have up to two additional terms on the right hand side of mass conservation equation. These terms quantify the rate of water entrainment (e.g. rainfall, infiltration, etc.) and the bed deformation. On the right hand side of momentum conservation equation two additional terms are added, which measure the effects of variable sediment concentration and momentum transfer due to sediment exchange between the water and movable bed ([8]). Examples of FCM can be found in [8, 23, 27, 3]. These models consider hydrostatic pressure. Unlike them, in [7] a non-hydrostatic system is used, in this kind of approach, special focus must be put in the appearances of numerical instabilities which are given by the non-hydrostatic distribution.

The PCM do not consider these additional terms in the shallow water equations because the sediment conservation and bed conservation are computed with the information provided by the hydrodynamics of clear water. Therefore, the interaction that may exist between the flux and sediment is ignored for the hydrodynamic equations. Examples of this kind of model can be found in [9] and [29]. In order to compute the morphological evolution, the majority of PCM do not take into account the bedload transport, although in works such as [36, 29], it is included.

The DM use the shallow water equations coupled with the bed conservation equation for modelling the sediment transport flux. The bed conservation, in this kind of model, presents a convective term that quantifies the bedload

transport. Examples of these models have been used in [1,10,31,24]. A summary of these different kinds of models can be seen in Table 1.

The first equation to model the bed balance was proposed by Felix Exner in his studies river morphology, [16,17]. In this equation, the sediment flux was approximated through flux velocity. In the currently literature different formulations are used to compute the bedload flux, for instance [30,14,21,40].

The majority of formulations proposed consider the critical Shields parameter, [35], to control the bed movement, nevertheless, the Grass law for bedload transport [21] does not consider this parameter, bed movement starts when the flux velocity is different to zero. The Grass law also allows measure if the interaction between bed and flux is strong or weak. In [10], a formulation where some bedload transport models are rewritten in analogous form to law of Grass, is proposed.

In order to solve numerically the sediment transport problem, several numerical strategies have been proposed. The majority of them are based on the finite volume numerical schemes, other strategies are based on cellular automata, although the use of cellular automata for modelling the sediment flux is a field that have been few explored, such as is pointed in [23]. As well, recently, the finite elements framework has been employed to compute the numerical solution of the sediment transport on shallow water equation, for instance [15,2,18] have employed this technique. Up to our knowledge the extension of approximate Riemann solvers is the most suitable option for the numerical resolution of the sediment transport, some one of them are exposed in [38] and [25].

In order to solve the complete system for sediment transport modelling, there are two means found in the literature, regardless of whether the model is FCM, PCM or DM. In the first one, the hyperbolic system of balance laws is solved through an approximate Riemann solver scheme. Then, the bed conservation equation is solved by using the information provided by this scheme. This method has been used in works like [8,23,31,24]. In the work [13] is discussed that this way to solve the sediment transport can fail due to the characteristic velocity related to the bedload is not taken into account for to solve the hydrodynamics of water sediment mixture. The second method computes the solution in coupled form, as in [27,3,28,29,33]. In order to compute the depth of bed together with the other variable the bed conservation equation is rewritten introducing a new conservative variable, which depends on the depth of bed and the suspended load.

According to Cao [8], the water flux, sediment transport and morphological evolution of the bed are strongly coupled. The rate of deformation can be significant in comparison with the flux evolution, then the use of a fully coupled model that takes into account all conservation laws is needed. In this paper, a FCM is considered, which takes into account both the suspended load sediment transport and the bedload sediment transport. The structure of this work is as follows: in section 2 the mathematical model is presented and the employed formulations for erosion and deposition are described. In section 3 a general compact formulation will be presented, as well as an alternative way

to write the model considering the presence of non conservative product ([10, 11]) and the study of the hyperbolicity of the model. The numerical schemes to be used will be shown in section 4, as well as the steady stationary solution which we want to preserve. Finally, in section 5 we validate the mathematical model and the numerical schemes by carrying out several numerical experiments and making comparison with between the obtained numerical results and the experimental data.

2 Mathematical model

In this work, an one-dimensional shallow water flow, over an erodible bottom composed of uniform, non-cohesive sediment, is analysed. This phenomenon is depicted in Figure 1.

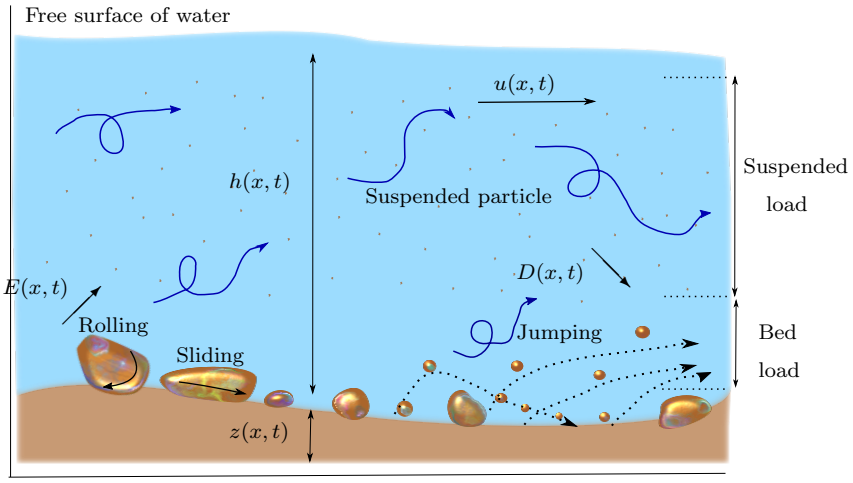

Fig. 1 Sketch of bedload and suspended-load sediment transport.

The dynamics of the movable bottom as a result of hydrodynamic behaviour can be modelled by using the system of balance laws made up by the mass conservation equation, the momentum conservation equation, the sediment conservation equation and the bed conservation equation, namely,

$$\frac{\partial h}{\partial t}(x,t) + \frac{\partial hu}{\partial x}(x,t) = \frac{E(x,t) - D(x,t)}{1-p}, \tag{1}$$

$$\begin{aligned}\frac{\partial(hu)}{\partial t}(x,t)+\frac{\partial\left(hu^2+\frac{1}{2}gh^2\right)}{\partial x}(x,t) = \; & gh(x,t)\left(-\frac{\partial z}{\partial x}(x,t)-S_f(x,t)\right)\\ & -\delta\frac{(\rho_s-\rho_w)gh^2(x,t)}{2\rho(x,t)}\frac{\partial c}{\partial x}(x,t)\\ & -\frac{(\rho_0-\rho(x,t))(E(x,t)-D(x,t))u(x,t)}{\rho(x,t)(1-p)},\end{aligned} \tag{2}$$

$$\frac{\partial(hc)}{\partial t}(x,t)+\frac{\partial(huc)}{\partial x}(x,t)=E(x,t)-D(x,t), \tag{3}$$

$$\frac{\partial z}{\partial t}(x,t)+\frac{1}{1-p}\frac{\partial q_b}{\partial x}(x,t)=\frac{D(x,t)-E(x,t)}{1-p}, \tag{4}$$

where

- $h(x,t)$ is the depth of water (m),
- $u(x,t)$ is the averaged-flux velocity (m/s),
- $c(x,t)$ is the averaged-flux volumetric sediment concentration (kg/m^3),
- $z(x,t)$ is the depth of bed (m),
- $\rho(x,t)$ is the density of water-sediment mixture (kg/m^3),
- $S_f(x,t)$ is the friction slope computed by using equation (8)),
- g is the gravitational acceleration (m/s^2),
- p is the bed sediment porosity,
- $E(x,t)$ is the sediment entrainment (m/s) (see [8]),
- $D(x,t)$ is the sediment deposition (m/s) (see [8]),
- ρ_w is the water density (kg/m^3),
- ρ_s is the sediment density (kg/m^3),
- ρ_0 is the saturated bed density (kg/m^3),
- $q_b(x,t)$ is the bed-load discharge (m^2/s) (see [21]).
- δ is defined as

$$\delta=\begin{cases}1 \text{ if } \theta \geqslant \theta_c,\\ 0 \text{ if } \theta < \theta_c,\end{cases} \tag{5}$$

  where θ and θ_c are the Shields parameter and Critical Shields value, respectively. These values are defined in section 2.1.

The right-hand site of the mass conservation law for the water sediment mixture (1), is significant for processes where the sediment transport and the morphological evolution are active (see [8]). The second term on the right-hand side of the momentum conservation equation (2), measures the effects of the variable sediment concentration on the flux direction. In [29] is pointed out that non-uniform sediment concentration over irregular bottom in quiescent water may cause perturbation of water at rest state, in order to deal with this issue, the second therm on the right hand is taken into account from the moment that the flux can move the bottom, it is mean, when the Shields parameter is greater than Critical Shield parameter. The third term represents the

momentum transfer due to the exchange between the water and the erodible bed, [8]. Equation (3) is the suspended sediment conservation equation. The morphodynamics are well-modelled by the Exner equation (4), which states that the time variation of the sediment layer, in a certain volume, is due to the net variation of the solid transport through of the boundaries of the volume, [16,17]. The formulation of the bed load discharge $q_b(x,t)$ can be based on empirical laws, some of these most often used were proposed in [30], [21] and [40]. In order to compute the bed load discharge, the law of Grass [21] was chosen for this work

$$q_b(x,t) = A_g u^3(x,t), \tag{6}$$

where A_g is a constant value that takes into account the diameter of the particle and the kinematic viscosity, usually it is obtained experimentally. The values for A_g range from zero to one, so that if A_g is close to zero, then the model shows a weak interaction between the sediment bottom and fluid. On the other hand, if A_g is close to one, then the interaction between the sediment bottom and fluid is strong, [10].

2.1 Morphological conditions

The density of the water-sediment mixture, ρ, and the density of the saturated bed, ρ_0, are computed as

$$\rho(x,t) = \rho_w(1 - c(x,t)) + \rho_s c(x,t) \quad \text{and} \quad \rho_0 = \rho_w p + \rho_s(1-p). \tag{7}$$

The friction term is computed using the following formula

$$S_f(x,t) = c_f u(x,t)|u(x,t)|, \tag{8}$$

where c_f is computed as

- $c_f = \dfrac{\eta^2}{h(x,t)^{\frac{4}{3}}}$, being η the dimensionless Manning coefficient.
- c_f is the friction coefficient.

The sediment exchange between the bed and the water column is determined through the sediment entrainment due to turbulence, $E(x,t)$, and the sediment deposition due to gravitational action, $D(x,t)$, (see [8]). The sediment entrainment is given by

$$E(x,t) = \begin{cases} \varphi \dfrac{(\theta(x,t) - \theta_c)u(x,t)}{h(x,t)d^{0.2}} & \text{if} \quad \theta(x,t) \geqslant \theta_c, \\ 0 & \text{else}, \end{cases} \tag{9}$$

the sediment deposition reads

$$D(x,t) = \alpha c(x,t)\omega_0(1 - \alpha c(x,t))^m, \tag{10}$$

where:

– φ is a constant dimensionless value determined by

$$\varphi = \phi \frac{560(1-p)\nu^{0.8}}{3(sg)^{0.4}\theta_c}. \tag{11}$$

This expression was deducted following to [8].
  – ϕ is a dimensionless value that depends on phenomenon to recreate,
  – ν is the kinematic viscosity of the fluid (m^2/s),
  – $s = \frac{\rho_s}{\rho_w} - 1$ is the submerged specific gravity of the sediment (kg/m^3),
  – θ_c is the dimensionless critical Shields parameter which indicates the start of sediment movement.

– The dimensionless Shields parameter or mobility parameter is computed using the formula

$$\theta(x,t) = \frac{u_*^2(x,t)}{sgd}, \tag{12}$$

where
  – d is the diameter of the particle (10^{-3} m),
  – $u_*(x,t)$ is the friction velocity (m/s), that is given by the relation

$$u_*(x,t) = \sqrt{\frac{\tau(x,t)}{\rho}},$$

  - $\tau(x,t)$ is the threshold stress of bottom computed using the following expression

$$\tau = \frac{g\rho\eta^2 u(x,t)|u(x,t)|}{h(x,t)^{1/3}}.$$

– The drop velocity ω_0(m/s) is computed using the formulation proposed in [42]

$$\omega_0 = \sqrt{\left(\frac{13.95\nu}{d}\right)^2 + 1.09sgd} - \frac{13.95\nu}{d}, \tag{13}$$

– m is an exponent computed by using the Reynolds number of the particle, see [26].

$$m = 4.45R^{-0.1} \quad \text{where,} \quad R = \frac{\omega_0 d}{\nu}. \tag{14}$$

– α is the nonequilibrium adaptation coefficient of suspended load, [41]. Following the work [8], this coefficient is defined by $\alpha = \min\{2, (1-p)/c\}$. This relation holds that near-bed supend-load concentration αc must be smaller than the bed material concentration $1-p$, [41].

In Table 1 are shown the different kinds of models which have been discussed in section 1, where the one dimensional shallow water equations are give by

$$\frac{\partial h}{\partial t}(x,t) + \frac{\partial hu}{\partial x}(x,t) = 0, \tag{15}$$

$$\frac{\partial hu}{\partial t}(x,t) + \frac{\partial hu^2 + \frac{1}{2}gh^2}{\partial x}(x,t) = -gh\frac{\partial z}{\partial x}(x,t). \tag{16}$$

Table 1 Model summary.

Model	Equations	Remarks
FCM	(1), (2), (3), (4)	Complete model used in this work
PCM	(15), (16), (3), (4)	Bedload discharge is neglected
DM	(15), (16), (4)	RHS of (4) is neglected

3 Problem statement

In order to write the mathematical model (1)-(3) in a compact manner the following notation is employed

- Conservative variables,
  - $w_1 = h(x,t)$ is the depth of water (m),
  - $w_2 = h(x,t)u(x,t)$ is the unit discharge (m^2/s),
  - $w_3 = h(x,t)c(x,t)$ is the suspended sediment concentration (kg/m^2),
  - $\mathbf{W}(x,t) := (w_1, w_2, w_3)^t$ is the vector of conservative variables.
- Physical flux,

$$\mathbf{F}(\mathbf{W}) = \begin{pmatrix} w_2 \\ \frac{w_2^2}{w_1} + \frac{1}{2}gw_1^2 \\ \frac{w_2 w_3}{w_1} \end{pmatrix}. \tag{17}$$

- Source term,

$$\mathbf{S}(x,t,\mathbf{W}) = \begin{pmatrix} \frac{E-D}{1-p} \\ -gw_1\left(\frac{\partial z}{\partial x} + S_f\right) - \frac{(\rho_s - \rho_w)gw_1^2}{2\rho}\frac{\partial}{\partial x}\left(\frac{w_3}{w_1}\right) - \frac{\rho_0 - \rho}{\rho}\frac{E-D}{1-p}\frac{w_2}{w_1} \\ E - D \end{pmatrix}. \tag{18}$$

The source term, $\mathbf{S}(x,t,\mathbf{W})$, is split into four parts: bed slope, $\mathbf{S}_1(x,t,\mathbf{W})$, friction slope, $\mathbf{S}_2(x,t,\mathbf{W})$, sediment entrainment and sediment deposition process, $\mathbf{S}_3(x,t,\mathbf{W})$, and volumetric sediment concentration slope,

$\mathbf{S}_4\,(x,t,\mathbf{W})$, so that:

$$\mathbf{S}(x,t,\mathbf{W}) = \sum_{K=1}^{4} \mathbf{S}_k(x,t,\mathbf{W}),$$

where

$$\mathbf{S}_1(x,t,\mathbf{W}) = \begin{pmatrix} 0 \\ -gw_{_1}\dfrac{\partial z}{\partial x}(x,t) \\ 0 \end{pmatrix}, \tag{19}$$

$$\mathbf{S}_2(x,t,\mathbf{W}) = \begin{pmatrix} 0 \\ -gw_{_1}S_f(x,t) \\ 0 \end{pmatrix}, \tag{20}$$

$$\mathbf{S}_3(x,t,\mathbf{W}) = \begin{pmatrix} \dfrac{E(x,t)-D(x,t)}{1-p} \\ -\dfrac{\rho_{_0}-\rho(x,t)}{\rho(x,t)}\dfrac{E(x,t)-D(x,t)}{1-p}\dfrac{w_{_2}}{w_{_1}} \\ E(x,t)-D(x,t) \end{pmatrix}, \tag{21}$$

and

$$\mathbf{S}_4(x,t,\mathbf{W}) = \begin{pmatrix} 0 \\ -gw_{_1}^2\dfrac{(\rho_s-\rho_w)}{2\rho(x,t)}\dfrac{\partial}{\partial x}\left(\dfrac{w_{_3}}{w_{_1}}\right) \\ 0 \end{pmatrix}. \tag{22}$$

Using this notation, the equations (1)-(3) can be rewritten in vectorial form as

$$\frac{\partial \mathbf{W}}{\partial t}(x,t) + \frac{\partial \mathbf{F}(\mathbf{W})}{\partial x}(x,t) = \mathbf{S}(x,t,\mathbf{W}), \tag{23}$$

for $x \in [0,\mathcal{L}]$ and $t \in [0,T]$, where $\mathcal{L}$ is the length of channel.

– Initial conditions:

$$\mathbf{W}(x,0) = \mathbf{W}_0(x), \quad \text{and} \quad z(x,0) = z_0(x), \quad x \in [0,\mathcal{L}].$$

In practice, the initial values for averaged depth of water $h_0(x)$, averaged flux velocity $u_0(x)$, averaged flux volumetric sediment concentration $c_0(x)$ and depth of bed $z_0(x)$, are known.

– Boundary conditions:
Conditions at the left end of the channel are detailed and the conditions of the right end are similar

– Inflow ($w_2(0,t) > 0$): $w_2(0,t) = q_l(t)$,
– Outflow ($w_2(0,t) < 0$): $w_2(0,t) = q_l(t)$,
– Wall $w_2(0,t) = 0$,
– Either inflow or outflow or wall: $w_1(0,t) = h_l(t)$ and $w_3(0,t) = h_l(t)c_l(t)$,

where $q_l(t)$, $h_l(t)$, $h_l(t)c_l(t)$ are the unit discharge, the depth of water and the suspended sediment concentration at time t, respectively, at left end of domain.

3.1 Hyperbolic character of the system

The balance law (23) can be written in quasi-linear form as

$$\frac{\partial \mathbf{W}}{\partial t}(x,t) + \mathbf{A}(\mathbf{W}(x,t))\frac{\partial \mathbf{W}}{\partial x}(x,t) = \mathbf{S}(x,t,\mathbf{W}), \tag{24}$$

where $\mathbf{A}(\mathbf{W}(x,t))$ is the Jacobian matrix of the physical flux $\mathbf{F}(\mathbf{W}(x,t))$, which is given by

$$\mathbf{A}(\mathbf{W}(x,t)) = \begin{pmatrix} 0 & 1 & 0 \\ gw_1 - \frac{w_2^2}{w_1^2} & 2\frac{w_2}{w_1} & 0 \\ -\frac{w_2 w_3}{w_1^2} & \frac{w_3}{w_1} & \frac{w_2}{w_1} \end{pmatrix}. \tag{25}$$

The eigenvalues of this matrix written as function of physical variable take the form:

$$\lambda_1 = u - \sqrt{gh},\ \lambda_2 = u,\ \lambda_3 = u + \sqrt{gh},$$

and the corresponding eigenvectors are:

$$\mathbf{v}_1 = \begin{pmatrix} 1 \\ \lambda_1 \\ c \end{pmatrix}, \qquad \mathbf{v}_2 = \begin{pmatrix} 0 \\ 0 \\ 1 \end{pmatrix}, \qquad \mathbf{v}_3 = \begin{pmatrix} 1 \\ \lambda_3 \\ c \end{pmatrix}.$$

3.2 Non conservative system

Due to that the derivative of conservative variables appears inside the source term $\mathbf{S}_4\,(x, t\mathbf{W},)$, then this source term can be seen as a non conservative product, [10]. Taken into account this fact, the hyperbolic system of conservation laws can be rewritten as

$$\frac{\partial \mathbf{W}}{\partial t} + \mathbf{A}(\mathbf{W})\frac{\partial \mathbf{W}}{\partial x} + \mathbf{B}(\mathbf{W})\frac{\partial \mathbf{W}}{\partial x} = \sum_{k=1}^{3} \mathbf{S}_k(x,t,\mathbf{W}). \tag{26}$$

The effects of the variable sediment concentration are taken into account in the third term on left-hand side of (26), also called the non conservative product. The matrix $\mathbf{B}(\mathbf{W})$ takes the form

$$\mathbf{B}(\mathbf{W}) = \begin{pmatrix} 0 & 0 & 0 \\ -gw_1\dfrac{\rho-\rho_w}{2\rho} & 0 & gw_1\dfrac{\rho_s-\rho_w}{2\rho} \\ 0 & 0 & 0 \end{pmatrix}. \tag{27}$$

3.2.1 Quasi linear form and hyperbolic character

The system of balance laws (26) can be written in quasi linear form as

$$\frac{\partial \mathbf{W}}{\partial t} + \mathcal{A}(\mathbf{W})\frac{\partial \mathbf{W}}{\partial x} = \sum_{k=1}^{3} \mathbf{S}_k(x,t,\mathbf{W}), \tag{28}$$

where

$$\mathcal{A}(\mathbf{W}) = \mathbf{A}(\mathbf{W}) + \mathbf{B}(\mathbf{W}) \tag{29}$$

and its eigenvalues are given by

$$\widetilde{\lambda}_1 = u - \sqrt{gh};\ \widetilde{\lambda}_2 = u;\ \widetilde{\lambda}_3 = u + \sqrt{gh},$$

and the associated eigenvectors are read

$$\widetilde{\mathbf{v}}_1 = \begin{pmatrix} 1 \\ \widetilde{\lambda}_1 \\ c \end{pmatrix}, \qquad \widetilde{\mathbf{v}}_2 = \begin{pmatrix} 1 \\ \widetilde{\lambda}_2 \\ \dfrac{\rho_w+\rho}{\rho_w-\rho_s} \end{pmatrix}, \qquad \widetilde{\mathbf{v}}_3 = \begin{pmatrix} 1 \\ \widetilde{\lambda}_3 \\ c \end{pmatrix},$$

Hence the system of partial differential equations (26) is strictly hyperbolic.

4 Numerical solution

In order to carry out the numerical resolution of the stated problem we need to solve numerically the hyperbolic system of balance laws (23) using a well balanced numerical scheme. Moreover, the posed problem involves to solve numerically the morphological evolution modelled by equation (4).

4.1 Problem discretization

We shall consider a uniform finite volume mesh over the interval $[0, \mathcal{L}] = [x_0, x_N]$, this mesh is shown in Figure 2. The i-th finite volume is denoted by

$$C_i = \left(x_{i-\frac{1}{2}}, x_{i+\frac{1}{2}}\right) = \left(x_i - \frac{x_i - x_{i-1}}{2}, x_i + \frac{x_{i+1} - x_i}{2}\right), \quad i = 1, \ldots, N-1,$$

where

$$x_i = i\Delta x, \quad \text{and} \quad \Delta x = \frac{\mathcal{L}}{N},$$

the boundary finite volumes are $C_0 = \left(x_0, x_{\frac{1}{2}}\right)$ and $C_N = \left(x_{N-\frac{1}{2}}, x_N\right)$.

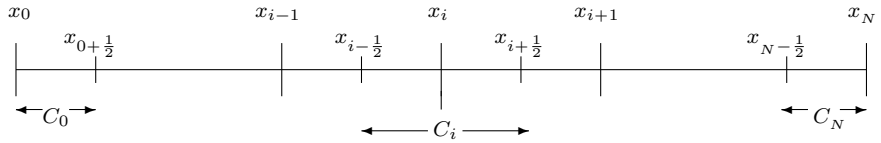

Fig. 2 Finite volume mesh: interior finite volume C_i, boundary finite volumes C_0 and C_N.

In order to get an approximate solution $\mathbf{W}(x, t_{n+1})$ of the exact solution $\mathbf{W}(x,t)$ at time t_{n+1}, we integrate (23) over arbitrary space-time rectangle $C_i \times [t_n, t^{n+1}]$:

$$\begin{aligned}\int_{C_i} \mathbf{W}(x, t^{n+1})dx \; &= \int_{C_i} \mathbf{W}(x, t^n)dx - \int_{t_n}^{t_{n+1}} \big(\mathbf{F}(\mathbf{W}(x_{i+1/2}, t)) \\ &\quad - \mathbf{F}(\mathbf{W}(x_{i-1/2}, t))\big)\, dt + \int_{t_n}^{t_{n+1}} \int_{C_i} \mathbf{S}(x, t, \mathbf{W}(x,t))dxdt.\end{aligned} \tag{30}$$

We shall denote by $\mathbf{W}_i^n$ the averaged approximate solution on the cell C_i at time t_n:

$$\mathbf{W}_i^n \cong \frac{1}{\Delta x} \int_{C_i} \mathbf{W}(x, t^n)dx, \tag{31}$$

then equation (30) takes the form

$$\begin{aligned}\mathbf{W}_i^{n+1} \; &= \mathbf{W}_i^n - \frac{1}{\Delta x} \int_{t_n}^{t_{n+1}} \big(\mathbf{F}(\mathbf{W}(x_{i+1/2}, t)) - \mathbf{F}(\mathbf{W}(x_{i-1/2}, t))\big)\, dt \\ &\quad + \int_{t_n}^{t_{n+1}} \mathbf{S}(x_i, t, \mathbf{W}_i^n)dt,\end{aligned} \tag{32}$$

where

$$\mathbf{S}(x_i, t, \mathbf{W}_i^n) := \frac{1}{\Delta x} \int_{C_i} \mathbf{S}(x, t, \mathbf{W}(x,t))dx. \tag{33}$$

4.2 Extension of the Q-scheme of van Leer

In this section we shall describe briefly the extension of the Q-scheme of van Leer, put forward in [5], in order to resolve (23).

4.2.1 Numerical flux

Due to the solution $\mathbf{W}(x,t_n)$ is defined by a piecewise function $\{\mathbf{W}_i^n\}_{i=1}^N$ then at the boundary of each finite volume cell, the values of the approximate solution are not well defined, so the integral of the physical flux cannot be computed at these points. For this reason, an approximation of the integral of physical flux, given by a function $\mathbf{\Phi}$, also called numerical flux is needed, so that

$$\frac{1}{\Delta t}\int_{t^n}^{t^{n+1}} \mathbf{F}(\mathbf{W}(x_{i+1/2},t))dt \approx \mathbf{F}^n_{i+\frac{1}{2}} := \mathbf{\Phi}(\mathbf{W}_i^n,\mathbf{W}_{i+1}^n), \qquad i=1,\dots N-1,$$

and

$$\frac{1}{\Delta t}\int_{t^n}^{t^{n+1}} \mathbf{F}(\mathbf{W}(x_{i-1/2},t))dt \approx \mathbf{F}^n_{i-\frac{1}{2}} := \mathbf{\Phi}(\mathbf{W}_{i-1}^n,\mathbf{W}_{i}^n), \qquad i=1,\dots N-1,$$

being $\Delta t = t_{n+1} - t_n$ the time step.

For the Q-scheme of van Leer the numerical flux $\mathbf{\Phi}$, takes the form

$$\mathbf{\Phi}(\mathbf{U},\mathbf{V}) = \frac{1}{2}\left(\mathbf{F}(\mathbf{U})+\mathbf{F}(\mathbf{V})\right) - \frac{1}{2}\left|\mathbf{Q}\left(\mathbf{U},\mathbf{V}\right)\right|\left(\mathbf{V}-\mathbf{U}\right), \tag{34}$$

with

$$\mathbf{Q}(\mathbf{U},\mathbf{V}) = \frac{\partial \mathbf{F}}{\partial \mathbf{W}}\left(\frac{1}{2}\left(\mathbf{U}+\mathbf{V}\right)\right).$$

The absolute value of a diagonalizable matrix $\mathbf{Q}$ is defined as follows: let $\mathbf{Q} = \mathbf{X}\mathbf{\Lambda}\mathbf{X}^{-1}$ where $\mathbf{\Lambda}$ is the diagonal matrix of the eigenvalues of $\mathbf{Q}$. Then $|\mathbf{Q}| = \mathbf{X}|\mathbf{\Lambda}|\mathbf{X}^{-1}$ where $|\mathbf{\Lambda}|$ is the diagonal matrix of the absolute value of the eigenvalues of $\mathbf{Q}$.

In order to avoid the loss of viscosity in the numerical scheme, the absolute value of the eigenvalues is redefined by using the Harten regularization, [22].

4.2.2 Numerical source terms

In this section is detailed the way as the approximation for the source term is computed.

Approximation of source terms: bed slope and sediment concentration slope Firstly, the discretization of both the bed slope source term and the sediment concentration slope source term, $\mathbf{S}^n_{1,i}$ and $\mathbf{S}^n_{4,i}$ respectively, are described. By extending the ideas put forward in [5], these source terms are approximated as

$$\mathbf{S}^n_{k,i} := \mathbf{\Psi}_{l,k}(x_{i-1}, x_i, t_n, \mathbf{W}^n_{i-1}, \mathbf{W}^n_i) + \mathbf{\Psi}_{r,k}(x_i, x_{i+1}, t_n, \mathbf{W}^n_i, \mathbf{W}^n_{i+1}), \quad k = 1 \text{ or } k = 4, \tag{35}$$

where

$$\mathbf{\Psi}_{l,k}(x, y, t, \mathbf{U}, \mathbf{V}) = \frac{1}{2}[\mathbf{I} + |\mathbf{Q}(\mathbf{U}, \mathbf{V})|\mathbf{Q}^{-1}(\mathbf{U}, \mathbf{V})]\ \widehat{\mathbf{S}}_k(x, y, t, \mathbf{U}, \mathbf{V}), \quad k = 1 \text{ or } k = 4,$$

and

$$\mathbf{\Psi}_{r,k}(y, z, t, \mathbf{V}, \mathbf{W}) = \frac{1}{2}[\mathbf{I} - |\mathbf{Q}(\mathbf{V}, \mathbf{W})|\mathbf{Q}^{-1}(\mathbf{V}, \mathbf{W})]\ \widehat{\mathbf{S}}_k(y, z, t, \mathbf{V}, \mathbf{W}), \quad k = 1 \text{ or } k = 4,$$

with

$$\widehat{\mathbf{S}}_1(x, y, t, \mathbf{U}, \mathbf{V}) := \begin{pmatrix} 0 \\ -g\dfrac{h(x,t) + h(y,t)}{2}\dfrac{\partial z}{\partial x}\left(\dfrac{x+y}{2}, t\right) \\ 0 \end{pmatrix} \tag{36}$$

and

$$\widehat{\mathbf{S}}_4(x, y, t, \mathbf{U}, \mathbf{V}) := \begin{pmatrix} 0 \\ -\delta g\left(\dfrac{h(x,t) + h(y,t)}{2}\right)^2 \dfrac{\rho_s - \rho_w}{\rho(x,t) + \rho(y,t)}\dfrac{\partial c}{\partial x}\left(\dfrac{x+y}{2}, t\right) \\ 0 \end{pmatrix}. \tag{37}$$

Approximation of friction slope source term The compute of the friction term is carry out as follows:

– Using a centred spatial discretization and an explicit time discretization, thus

$$\mathbf{S}^n_{2,i} = \begin{pmatrix} 0 \\ -g\dfrac{\eta^2 w^n_{2,i}|w^n_{2,i}|}{(w^n_{1,i})^{(7/3)}} \\ 0 \end{pmatrix}. \tag{38}$$

– Using a centred spatial discretization and a semi-implicit time discritization so the friction source term reads

$$\mathbf{S}_{2,i}^{n} = \begin{pmatrix} 0 \\ -g\dfrac{\eta^2 w_{2,i}^{n+1}|w_{2,i}^{n}|}{(w_{1,i}^{n})^{(7/3)}} \\ 0 \end{pmatrix}. \tag{39}$$

Approximation of the sediment entrainment and sediment deposition processes source terms Variables in the source term $\mathbf{S}_3(x,t,\mathbf{W}(x,t))$ are evaluated pointwise in the node i at time t_n, therefore

$$\mathbf{S}_{3,i}^{n} = \begin{pmatrix} \dfrac{E_i^n - D_i^n}{1-p} \\ -\dfrac{\rho_0-\rho}{\rho}\dfrac{E_i^n - D_i^n}{1-p}\dfrac{w_{2,i}^n}{w_{1,i}^n} \\ E_i^n - D_i^n \end{pmatrix}, \tag{40}$$

where $E_i^n = E(x_i,t_n)$ and $D_i^n = D(x_i,t_n)$ whose expressions are given by (9) and (10), respectively.

Therefore the extension of Q-scheme of van Leer to compute the approximate solution of the hyperbolic system of balance laws (23) takes the form

$$\mathbf{W}_i^{n+1} = \mathbf{W}_i^n - \frac{\Delta t}{\Delta x}\left(\mathbf{F}_{i+\frac{1}{2}}^n - \mathbf{F}_{i-\frac{1}{2}}^n\right) + \Delta t \sum_{k=1}^{4} \mathbf{S}_{k,i}^n. \tag{41}$$

where the numerical flux is defined by (34) and the source term discretizations are given by (35), (38), (39) and (40).

4.3 HLLCS scheme

The second scheme to compute the numerical solution for the hyperbolic system of balance laws (23) is the HLLCS approximate Riemann solver, [32]. This scheme is based in the HLLC approximate Riemann solver [39], but the source terms $\mathbf{S}_1(x,t,\mathbf{W})$ and $\mathbf{S}_2(x,t,\mathbf{W})$ are taken into account inside the numerical flux.

4.3.1 Numerical flux

Borrowing from the work [32], in order to include the bed slope source term and the friction slope source term inside the numerical flux, the Rankine-Hugoniot

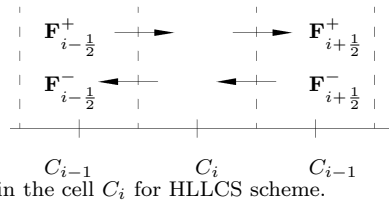

Fig. 3 Numerical flux in the cell C_i for HLLCS scheme.

relation for steady shock, of shock speed $\mathcal{S}$, at $x = 0$ and $t = 0$ is followed, namely,

$$\begin{aligned}\mathbf{F}^+(\mathbf{W}(x_{i+1},t)) \; - \mathbf{F}^-(\mathbf{W}(x_i,t)) - \sum_{k=1}^{2} \bar{\mathbf{S}}_k \left(x_{i+\frac{1}{2}}, t, \mathbf{W}(x_{i+\frac{1}{2}},t)\right) \\ = \mathcal{S}\left(\mathbf{W}^+(x_{i+1},t) - \mathbf{W}^-(x_i,t)\right) = 0,\end{aligned} \tag{42}$$

where $\bar{\mathbf{S}}_k$ $(k = 1, 2)$, is the averaged approximated source term at $x = 0$ and $t = 0$, so that

$$\sum_{k=1}^{2} \bar{\mathbf{S}}_k(x_{i+\frac{1}{2}}, t, \mathbf{W}(x_{i+\frac{1}{2}},t)) = \begin{bmatrix} \bar{\mathscr{S}}_1 \\ \bar{\mathscr{S}}_2 \\ \bar{\mathscr{S}}_3 \end{bmatrix}. \tag{43}$$

Due to the source terms $\bar{\mathbf{S}}_1(x,t,\mathbf{W})$ and $\bar{\mathbf{S}}_2(x,t,\mathbf{W})$ are taken into account inside the numerical flux, the hyperbolic system of balance laws (23) can be solved by using the numerical scheme

$$\begin{aligned}\mathbf{W}(x_i,t_{n+1}) = \mathbf{W}(x_i,t_n) - \frac{\Delta t}{\Delta x}\left(\mathbf{F}^{HLLCS-}_{i+\frac{1}{2}} - \mathbf{F}^{HLLCS+}_{i-\frac{1}{2}}\right) \\ + \Delta t \sum_{k=3}^{4} \mathbf{S}_k\left(x_i, t_n, \mathbf{W}(x_i,t_n)\right),\end{aligned} \tag{44}$$

where $\mathbf{F}^{HLLCS\pm}_{i\pm\frac{1}{2}}$ are the numerical flows with the source terms inside it. The contributions made by the numerical flux in the cells depends on the sign of the eigenvalues at the boundaries, see Figure 3.

In order to define the numerical flux we need to have established values λ_i, λ_{i+1}, and $\lambda^{\pm}_{*}$, which represent a middle wave related to the source terms $\bar{\mathbf{S}}_1$ and $\bar{\mathbf{S}}_2$, see Figure 4. These values are given by expressions (49)-(53).

In order to compute the numerical flux, we shall extend for the bottom variations the work done in [32], where the numerical flux is computed as:

– If $0 \leqslant \lambda_i$, then

$$\begin{aligned}\mathbf{F}^{HLLCS-}_{i+\frac{1}{2}} &= \mathbf{F}(\mathbf{W}(x_i,t)), \\ \mathbf{F}^{HLLCS+}_{i+\frac{1}{2}} &= \mathbf{F}(\mathbf{W}(x_i,t)) + \sum_{k=1}^{2} \bar{\mathbf{S}}_k(x_{i+\frac{1}{2}}, t, \mathbf{W}(x_{i+\frac{1}{2}},t)).\end{aligned} \tag{45}$$

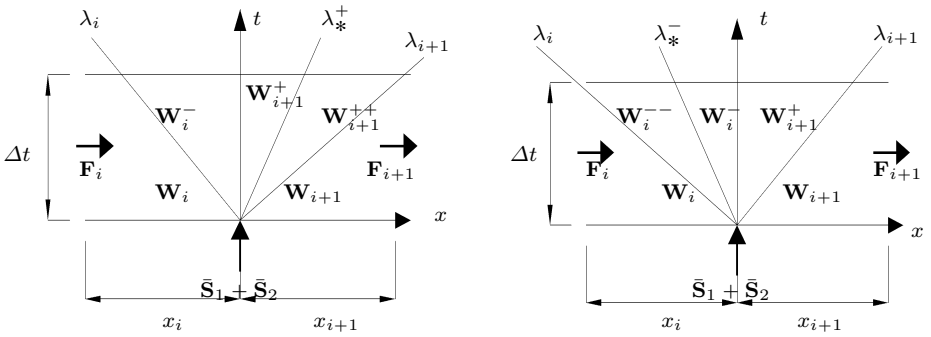

(a) Positive middle wave. (b) Negative middle wave.

Fig. 4 HLLCS numerical flux.

– If $0 \geqslant \lambda_{i+1}$, then

$$\begin{aligned} \mathbf{F}_{i+\frac{1}{2}}^{HLLCS-} &= \mathbf{F}(\mathbf{W}(x_{i+1},t)) - \sum_{k=1}^{2} \bar{\mathbf{S}}_k(x_{i+\frac{1}{2}},t,\mathbf{W}(x_{i+\frac{1}{2}},t)), \\ \mathbf{F}_{i+\frac{1}{2}}^{HLLCS+} &= \mathbf{F}(\mathbf{W}(x_{i+1},t)). \end{aligned} \tag{46}$$

– If $\lambda_i \leqslant 0 \leqslant \lambda_{i+1}$, then
  – if $\lambda_*^+ > 0$, then

$$\begin{aligned} \mathbf{F}_{i+\frac{1}{2}}^{HLLCS-} &= \mathbf{F}(\mathbf{W}(x_i,t)) + \lambda_i(\mathbf{W}^-(x_i,t) - \mathbf{W}(x_i,t)), \\ \mathbf{F}_{i+\frac{1}{2}}^{HLLCS+} &= \mathbf{F}_{i+\frac{1}{2}}^{HLLCS-} + \sum_{k=1}^{2} \bar{\mathbf{S}}_k(x_{i+\frac{1}{2}},t,\mathbf{W}(x_{i+\frac{1}{2}},t)), \end{aligned} \tag{47}$$

where

$$\mathbf{W}^-(x_i,t) = \mathbf{W}^+(x_{i+1},t) - \bar{\mathbf{H}}_{i+\frac{1}{2}}^+,$$

$$\bar{\mathbf{H}}_{i+\frac{1}{2}}^+ = -\frac{\bar{\mathscr{I}}_2}{\widetilde{\lambda}_1\widetilde{\lambda}_2}\begin{pmatrix} 1 \\ 0 \\ c(x_i,t) \end{pmatrix}, \quad \mathbf{W}^+(x_{i+1},t) = w_{1,i+1}^+\begin{pmatrix} 1 \\ \lambda_*^+ \\ c(x_i,t) \end{pmatrix},$$

and

$$w_{1,i+1}^+ = \left(\frac{(w_{1,i})\,(u_i - \lambda_i) - \lambda_i \bar{H}_{i+\frac{1}{2},1}^+}{\lambda_*^+ - \lambda_i}\right).$$

  – If $\lambda_*^- < 0$, then

$$\begin{aligned} \mathbf{F}_{i+1/2}^{HLLCS-} &= \mathbf{F}(\mathbf{W}(x_{i+1},t)) + \lambda_{i+1}(\mathbf{W}^+(x_{i+1},t) - \mathbf{W}(x_{i+1},t)), \\ \mathbf{F}_{i+1/2}^{HLLCS+} &= \mathbf{F}_{i+1/2}^{HLLCS-} - \sum_{k=1}^{2} \bar{\mathbf{S}}_k(x_{i+\frac{1}{2}},t,\mathbf{W}(x_{i+\frac{1}{2}},t)), \end{aligned} \tag{48}$$

where

$$\mathbf{W}^{+}(x_{i+1},t) = \mathbf{W}^{-}(x_i,t) + \bar{\mathbf{H}}^{-}_{i+\frac{1}{2}},$$

$$\bar{\mathbf{H}}^{-}_{i+\frac{1}{2}} = -\frac{\bar{\mathscr{S}_2}}{\widetilde{\lambda}_1\widetilde{\lambda}_2}\begin{pmatrix}1\\0\\c(x_{i+1},t)\end{pmatrix}, \quad \mathbf{W}^{-}(x_i,t) = w^{-}_{1,i}\begin{pmatrix}1\\\lambda^{-}_{*}\\c(x_{i+1},t)\end{pmatrix},$$

and

$$w^{-}_{1,i} = \left(\frac{w_{1,i+1}\left(u_{i+1}-\lambda_{i+1}\right) - \lambda_{i+1}\bar{H}^{-}_{i+\frac{1}{2},1}}{\lambda^{-}_{*}-\lambda_{i+1}}\right).$$

The values λ_i, λ_{i+1} are given by the following expression:

$$\lambda_i = \begin{cases}\min\left\{\widetilde{\lambda}_1;\, u_i - \sqrt{g w_{1,i}};\, u_{i+1} - \sqrt{g w_{1,i+1}}\right\} & \text{if} \quad |\mathscr{S}_2| = 0,\\ \widetilde{\lambda}_1 & \text{if} \quad |\mathscr{S}_2| \neq 0.\end{cases} \tag{49}$$

$$\lambda_{i+1} = \begin{cases}\max\left\{\widetilde{\lambda}_2;\, u_i + \sqrt{g w_{1,i}};\, u_{i+1} + \sqrt{g w_{1,i+1}}\right\} & \text{if} \quad |\mathscr{S}_2| = 0,\\ \widetilde{\lambda}_2 & \text{if} \quad |\mathscr{S}_2| \neq 0.\end{cases} \tag{50}$$

The average values $\widetilde{\lambda}_1$ and $\widetilde{\lambda}_2$ are the Roe mean [34], with expressions (51)

$$\widetilde{u} = \frac{u_i\sqrt{w_{1,i}} + u_{i+1}\sqrt{w_{1,i+1}}}{\sqrt{w_{1,i}} + \sqrt{w_{1,i+1}}} \tag{51}$$

and,

$$\widetilde{\lambda}_1 = \widetilde{u} - \sqrt{g\frac{w_{1,i}+w_{1,i+1}}{2}}, \quad \widetilde{\lambda}_2 = \widetilde{u} + \sqrt{g\frac{w_{1,i}+w_{1,i+1}}{2}},$$

Finally the values for $\lambda^{\pm}_{*}$ take the form

$$\lambda^{+}_{*} = \frac{\lambda_i w_{1,i+1}\left(u_{i+1}-\lambda_{i+1}\right) - \lambda_{i+1}w_{1,i}\left(u_i-\lambda_i\right) + \lambda_{i+1}(\lambda_i\bar{H}^{+}_{i+\frac{1}{2},1} - \mathscr{S}_1)}{w_{1,i+1}\left(u_{i+1}-\lambda_{i+1}\right) - w_{1,i}\left(u_i-\lambda_i\right) + \lambda_i\bar{H}^{+}_{i+\frac{1}{2},1}}, \tag{52}$$

and

$$\lambda^{-}_{*} = \frac{\lambda_i w_{1,i+1}\left(u_{i+1}-\lambda_{i+1}\right) - \lambda_{i+1}w_{1,i}\left(u_i-\lambda_i\right) + \lambda_{i+1}(\lambda_i\bar{H}^{-}_{i+\frac{1}{2},1} - \mathscr{S}_1)}{w_{1,i+1}\left(u_{i+1}-\lambda_{i+1}\right) - w_{1,i}\left(u_i-\lambda_i\right) + \lambda_i\bar{H}^{-}_{i+\frac{1}{2},1}}. \tag{53}$$

4.3.2 Bed slope approximation

In order to get fully described the discretization of bed slope source term, we shall follow to [32], where the approximation for the bed slope is given by

$$\frac{\partial z}{\partial x}(x_{i+\frac{1}{2}}, t_n) \approx \frac{g}{\Delta x}\left(w_{1,j}^n - \frac{|\delta z'|}{2}\right)\delta z', \tag{54}$$

where

$$j = \begin{cases} i & \text{if } \delta z \geqslant 0, \\ i+1 & \text{if } \delta z < 0, \end{cases} \quad \text{and} \quad \delta z' = \begin{cases} w_{1,i}^n & \text{if } \delta z \geqslant 0 \text{ and } d_i < z_{i+1}^n, \\ w_{1,i+1}^n & \text{if } \delta z < 0 \text{ and } d_{i+1} < z_i^n, \\ \delta z & \text{else,} \end{cases}$$

being $\delta z = z(x_{i+1}, t_n) - z(x_i, t_n)$ and $d_i = w_1(x_i, t_n) + z(x_i, t_n)$.

4.3.3 Friction term approximation

The friction term is approximated by using the following relation, (see [32]).

$$\left|\frac{S_f}{g\widetilde{w}_1}\Delta x\right|_{i+\frac{1}{2}} = \min\left(\left|\frac{S_f}{g\widetilde{w}_1}\Delta x\right|, \left|\widetilde{u}\frac{|u_{\min}|}{2g}\right|\right)_{i+\frac{1}{2}}, \tag{55}$$

where

$$|u_{\min}| = \min\left(|u_i|, |u_{i+1}|\right), \tag{56}$$

and S_f is computing using equation (8) by choosing c_f as the friction coefficient.

4.3.4 Approximation of sediment concentration slope, sediment erosion and sediment deposition process

The source terms $\mathbf{S}_3(x,t)$ and $\mathbf{S}_4(x,t)$ in the numerical scheme (44) are approximated as follows

$$\sum_{k=3}^{4}\mathbf{S}_{k,i}^n = \begin{pmatrix} \dfrac{E_i^n - D_i^n}{1-p} \\ -\delta g w_{1,i}^2 \dfrac{\rho_s - \rho_w}{2\rho_i}\dfrac{c_i^n - c_{i-1}^n}{\Delta x} - \dfrac{\rho_0 - \rho}{\rho}\dfrac{E_i^n - D_i^n}{1-p}u_i^n \\ E_i^n - D_i^n \end{pmatrix}. \tag{57}$$

4.4 Numerical scheme for the non-conservative system

In order to deal with the presences of non conservative products, a suitable numerical treatment of them is needed. Following [10] the numerical solution of (26) at cell C_i at time t_n is computed using a numerical scheme of the form

$$\begin{aligned}\mathbf{W}_i^{n+1} = \mathbf{W}_i^n - \frac{\Delta t}{\Delta x}\Big(&\mathcal{A}_{\mathcal{D}}^{+}\left(\mathbf{W}_{i-\frac{1}{2}}^n\right)\left(\mathbf{W}_i^n - \mathbf{W}_{i-1}^n\right) \\ &+ \mathcal{A}_{\mathcal{D}}^{-}\left(\mathbf{W}_{i+\frac{1}{2}}^n\right)\left(\mathbf{W}_{i+1}^n - \mathbf{W}_i^n\right)\Big) + \Delta t \sum_{k=1}^{3} \mathbf{S}_{k,i}^n,\end{aligned} \tag{58}$$

where

$$\mathcal{A}_{\mathcal{D}}^{\pm}\left(\mathbf{W}_{i+\frac{1}{2}}\right) = \frac{1}{2}\left(\mathcal{A}\left(\mathbf{W}_{i+\frac{1}{2}}\right) \pm \left|\mathcal{A}\left(\mathbf{W}_{i+\frac{1}{2}}\right)\right|\right),$$

Taking into account the definition of $\mathcal{A}$ given by equation (29) the numerical scheme (58) becomes in

$$\begin{aligned}\mathbf{W}_i^{n+1} = \ &\mathbf{W}_i^n - \frac{\Delta t}{\Delta x}\left(\mathcal{G}_{i+\frac{1}{2}}^n - \mathcal{G}_{i-\frac{1}{2}}^n\right) \\ &- \frac{\Delta t}{2\Delta x}\left(\mathbf{B}\left(\mathbf{W}_{i+\frac{1}{2}}^n\right)\left(\mathbf{W}_{i+1}^n - \mathbf{W}_i^n\right) + \mathbf{B}\left(\mathbf{W}_{i-\frac{1}{2}}^n\right)\left(\mathbf{W}_i^n - \mathbf{W}_{i-1}^n\right)\right) \\ &+ \Delta t \sum_{k=1}^{3} \mathbf{S}_{k,i}^n\end{aligned} \tag{59}$$

where

$$\mathcal{G}_{i+\frac{1}{2}}^n = \frac{1}{2}\left(\mathbf{F}(\mathbf{W}_{i+1}^n) + \mathbf{F}(\mathbf{W}_i^n)\right) - \frac{1}{2}\left|\mathcal{A}\left(\mathbf{W}_{i+\frac{1}{2}}^n\right)\right|\left(\mathbf{W}_{i+1}^n - \mathbf{W}_i^n\right). \tag{60}$$

The discretization of the bed slope source term $\mathbf{S}_1(x,t)$ is carried out following the methodology explained in section 4.2.2, but in this case the upwind process is done with regard to the eigenvalues of matrix $\mathcal{A}$.

The source term, which contains the friction slope $\mathbf{S}_2(x,t)$, is discretized by using either, (38) or (39) while the source term that takes into account the sediment entrainment and deposition processes $\mathbf{S}_3(x,ts)$, is discretized by using (40).

4.5 Morphological evolution

Exner equation (4) is not actually hyperbolic, however it is possible to write a wave speed estimation $\widetilde{\lambda}_b$ associated to sediment flux (see [24]), such that the Exner equation becomes in

$$\frac{\partial z}{\partial t}(x,t) + \widetilde{\lambda}_b \frac{\partial z}{\partial x}(x,t) = \frac{D(x,t) - E(x,t)}{1-p}, \tag{61}$$

where

$$\widetilde{\lambda}_b = \frac{1}{1-p}\frac{\partial q_b}{\partial z}, \tag{62}$$

this wave speed is the basis to build an upwind strategy to solve the morphological evolution.

In order to solve the Exner equation (4), we integrate that equation over a space-time arbitrary rectangle $C_i \times [t_n, t_n + 1]$, as it was done in section 4.1.

$$z_i^{n+1} = z_i^n + \frac{\Delta t}{1-p}\left(D_i^n - E_i^n\right) - \frac{1}{\Delta x}\int_{t_n}^{t_{n+1}} \frac{1}{1-p}\left(q_b(x_{i+\frac{1}{2}}, t) - q_b(x_{i-\frac{1}{2}}, t)\right) dt. \tag{63}$$

Following the finite volume methodology, an approximation $q^n_{b,i\pm\frac{1}{2}}$ for the integral of bedload discharge at the common boundary $x_{i\pm\frac{1}{2}}$ between two finite volume cells, is needed, namely

$$q^n_{b,i\pm\frac{1}{2}} \approx \frac{1}{\Delta t}\int_{t_n}^{t_{n+1}} q_b(x_{i\pm\frac{1}{2}}, t)dt. \tag{64}$$

Following [24], this approximation is defined as follows

$$\begin{aligned} q^n_{_{b,i+\frac{1}{2}}} &:= \begin{cases} q_b(x_i, t_n) & \text{if } \widetilde{\lambda}_{b,i+\frac{1}{2}} > 0, \\ q_b(x_{i+1}, t_n) & \text{if } \widetilde{\lambda}_{b,i+\frac{1}{2}} < 0, \end{cases} \\ q^n_{_{b,i-\frac{1}{2}}} &:= \begin{cases} q_b(x_{i-1}, t_n) & \text{if } \widetilde{\lambda}_{b,i-\frac{1}{2}} > 0, \\ q_b(x_i, t_n) & \text{if } \widetilde{\lambda}_{b,i-\frac{1}{2}} < 0, \end{cases} \end{aligned} \tag{65}$$

where

$$\widetilde{\lambda}_{b,i+\frac{1}{2}} = \frac{1}{1-p}\frac{q_b(x_{i+1}, t_n) - q_b(x_i, t_n)}{z(x_{i+1}, t_n) - z(x_i, t_n)}. \tag{66}$$

Finally, the scheme to solve the Exner equation (4) reads

$$z_i^{n+1} = z_i^n + \frac{\Delta t}{1-p}\left(D_i^n - E_i^n - \frac{1}{\Delta x}\left(q^n_{_{b,i+\frac{1}{2}}} - q^n_{_{b,i-\frac{1}{2}}}\right)\right). \tag{67}$$

4.6 Numerical treatment of boundary conditions

The numerical methods described earlier are applied to internal cells, C_i, $i = 1, \ldots, N-1$. At the boundary cells we cannot use these methods because for boundaries nodes $x_B = x_0$ or $x_B = x_N$, left or right neighbouring nodes, which are necessary to define the numerical flux or upwind the source term, do not exist.

So as to compute the values of conservative variables at the boundaries, fictitious neighbouring nodes $\widehat{x}_B$ (see [4]) or ghost cells C_B, (see[25]), are introduced, see Figure 4.6.

The values of the conservative variables in these cells are defined according to the boundary conditions, which can be either inflow, outflow or wall. For

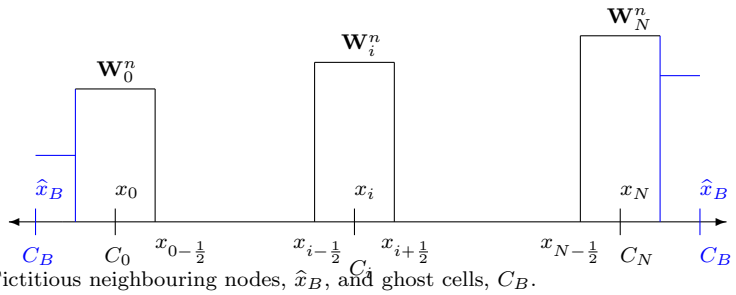

Fig. 5 Fictitious neighbouring nodes, $\widehat{x}_B$, and ghost cells, C_B.

each case, the values of the conservative variables on fictitious neighbouring nodes are:

- Inflow ($w_{0,2} > 0$ or $w_{N,2} < 0$)
  - Left end: $\mathbf{W}(\widehat{x}_B, t_n) = \mathbf{W}(x_0, t_n)$, $z(\widehat{x}_B, t_n) = z(x_0, t_n)$,
  - Right end: $\mathbf{W}(\widehat{x}_B, t_n) = \mathbf{W}(x_N, t_n)$, $z(\widehat{x}_B, t_n) = z(x_N, t_n)$.
- Outflow ($w_{0,2} < 0$ or $w_{N,2} > 0$)
  - Left end: $\mathbf{W}(\widehat{x}_B, t_n) = \mathbf{W}(x_0, t_n)$, $z(\widehat{x}_B, t_n) = z(x_0, t_n)$,
  - Right end: $\mathbf{W}(\widehat{x}_B, t_n) = \mathbf{W}(x_N, t_n)$, $z(\widehat{x}_B, t_n) = z(x_N, t_n)$.
- Wall ($w_{0,2} = 0$ or $w_{N,2} = 0$)
  - Left end: $w_1(\widehat{x}_B, t_n) = w_1(x_0, t_n)$, $w_2(\widehat{x}_B, t_n) = -w_2(x_0, t_n)$, $w_3(\widehat{x}_B, t_n) = w_3(x_0, t_n)$, $z(\widehat{x}_B, t_n) = z(x_0, t_n)$,
  - Right end: $w_1(\widehat{x}_B, t_n) = w_1(x_N, t_n)$, $w_2(\widehat{x}_B, t_n) = -w_2(x_N, t_n)$, $w_3(\widehat{x}_B, t_n) = w_3(x_N, t_n)$, $z(\widehat{x}_B, t_n) = z(x_N, t_n)$.

The approximate solution at the boundaries is computed by using the values of the conservative variables on ghost cells and either of the numerical schemes described earlier.

4.7 Steady stationary solution

A numerical scheme is called well balanced if it can preserve a family of stationary solution. For that reason the study of the stationary solution is important. In order to get the steady-stationary solution for the system of balance laws (23) and (4), let us suppose that $u(x,t) = 0$, in this case $\theta < \theta_c$, then the system of balance laws reduces to

$$\frac{\partial h}{\partial t}(x,t) = \frac{-1}{1-p} D(x,t), \tag{68}$$

$$\frac{\partial h}{\partial x}(x,t) + \frac{\partial z}{\partial x}(x,t) = 0, \tag{69}$$

$$\frac{\partial hc}{\partial t}(x,t) = -D(x,t), \tag{70}$$

$$\frac{\partial z}{\partial t}(x,t) = \frac{1}{1-p} D(x,t). \tag{71}$$

From equations (68) and (71) we can see that both, the depth of water and the depth of the bottom may vary, but the free surface of water $\varsigma(x,t) = h(x,t) + z(x,t)$ stays constant with respect of time, namely

$$\frac{\partial \varsigma}{\partial t}(x,t) = \frac{\partial h}{\partial t}(x,t) + \frac{\partial z}{\partial t}(x,t) = 0. \tag{72}$$

Therefore, from (69) and (72) is concluded that the free surface of water is a constant with respect of time and space.

From equation (70) and by using (68), we get

$$\frac{\partial c}{\partial t}(x,t) = \frac{D(x,t)}{h(x,t)} \left(\frac{c(x,t)}{1-p} - 1 \right). \tag{73}$$

This equation shows that the variation of the volumentric sediment concentration over time is equal to zero if either $D(x,t) = 0$ then $c(x,t) = 0$ or $c(x,t) = 1-p$. Moreover if $c(x,t) < 1-p$ then $c(x,t)$ is a decreasing function over time.

Definition 1 *The steady stationary solution of balance laws system (23) and (4) is given by the follows conditions*

- *The water free surface is a constant function, see equations (69) and (72).*
- *Null velocity in the whole domain, $u = 0$.*
- *The variation of suspended sediment concentration over time is equal to the opposite of deposition, see equation (70).*

Proposition 1 *Let us suppose that $\mathbf{W}(x_i, t_n)$ and $z(x_i, t_n)$ fulfill the steady stationary solutions conditions, then the numerical scheme defined by equations (41), (34), (35), either (38) or (39), (40) and (67), computes the steady stationary solutions conditions exactly, that is mean*

- *The free surface is constant.*
- *The velocity is null over whole domain.*
- *The suspended sediment concentration variation with respect to time is equal to opposite of deposition.*

Proof The values for the different variables at interface $x_{i\pm 1/2}$ will be computed as the arithmetic mean. Under water at rest hypothesis, the different elements of numerical scheme take the following forms:

– Convective discretization,

$$\begin{aligned}&\frac{1}{\Delta x}(\mathbf{F}^n_{i+\frac{1}{2}} - \mathbf{F}^n_{i-\frac{1}{2}})\\ &= \begin{pmatrix} \dfrac{w^n_{1,i} - w^n_{1,i-1}}{2\Delta x}\sqrt{g\, w^n_{1,i-\frac{1}{2}}} - \dfrac{w^n_{1,i+1} - w^n_{1,i}}{2\Delta x}\sqrt{g\, w^n_{1,i+\frac{1}{2}}} \\ \dfrac{g}{4\Delta x}\left((w^n_{1,i+1})^2 - (w^n_{1,i-1})^2\right) \\ c^n_{i-\frac{1}{2}}\dfrac{w^n_{1,i} - w^n_{1,i-1}}{2\Delta x}\sqrt{g\, w^n_{1,i-\frac{1}{2}}} - c^n_{i+\frac{1}{2}}\dfrac{w^n_{1,i+1} - w^n_{1,i}}{2\Delta x}\sqrt{g\, w^n_{1,i+\frac{1}{2}}} \end{pmatrix}.\end{aligned} \tag{74}$$

– Discretization of bed slope source term,

$$\mathbf{S}^n_{1,i} = \begin{pmatrix} \dfrac{1}{2}\dfrac{z^n_{i+1} - z^n_i}{\Delta x}\sqrt{g\, w^n_{1,i+\frac{1}{2}}} - \dfrac{1}{2}\dfrac{z^n_i - z^n_{i-1}}{\Delta x}\sqrt{g\, w^n_{1,i-\frac{1}{2}}} \\ -\dfrac{g}{2}w_{1,i+\frac{1}{2}}\dfrac{z^n_{i+1} - z^n_i}{\Delta x} - \dfrac{g}{2}w^n_{1,i-\frac{1}{2}}\dfrac{z^n_i - z^n_{i-1}}{\Delta x} \\ \dfrac{1}{2}c_{i+\frac{1}{2}}\sqrt{g\, w^n_{1,i+\frac{1}{2}}}\dfrac{z^n_{i+1} - z^n_i}{\Delta x} - \dfrac{1}{2}c_{i-\frac{1}{2}}\sqrt{g\, w^n_{1,i-\frac{1}{2}}}\dfrac{z^n_i - z^n_{i-1}}{\Delta x} \end{pmatrix}. \tag{75}$$

– Discretization of friction slope source term, $\mathbf{S}^n_{2,i} = \mathbf{0}$.

– Discretization of sediment entrainment and sediment deposition process source term,

$$\mathbf{S}^n_{3,i} = \begin{pmatrix} \dfrac{-D^n_i}{1-p} \\ 0 \\ -D^n_i \end{pmatrix}. \tag{76}$$

– Discretization of sediment concentration slope source term,

$$\mathbf{S}^n_{4,i} = \delta \begin{pmatrix} S^n_{(4,i),1} \\ S^n_{(4,i),2} \\ S^n_{(4,i),3} \end{pmatrix}, \tag{77}$$

where

$$\begin{aligned}S^n_{(4,i),1} = &\frac{1}{2}\frac{c^n_{i+1} - c^n_i}{\Delta x}\sqrt{g\, w^n_{1,i+\frac{1}{2}}}\, w^n_{1,i+\frac{1}{2}}\frac{\rho_s - \rho_w}{2\rho^n_{i+\frac{1}{2}}}\\ &- \frac{1}{2}\frac{c^n_i - c^n_{i-1}}{\Delta x}\sqrt{g\, w^n_{1,i-\frac{1}{2}}}\, w^n_{1,i-\frac{1}{2}}\frac{\rho_s - \rho_w}{2\rho^n_{i-\frac{1}{2}}},\end{aligned}$$

$$S^n_{(4,i),2} = -\frac{g}{2}\frac{c^n_{i+1}-c^n_i}{\Delta x}\left(w^n_{1,i+\frac{1}{2}}\right)^2\frac{\rho_s-\rho_w}{2\rho^n_{i+\frac{1}{2}}} - \frac{g}{2}\frac{c^n_i-c^n_{i-1}}{\Delta x}\left(w^n_{1,i-\frac{1}{2}}\right)^2\frac{\rho_s-\rho_w}{2\rho^n_{i-\frac{1}{2}}},$$

$$S^n_{(4,i),3} = \frac{1}{2}\frac{c^n_{i+1}-c^n_i}{\Delta x}c^n_{1+\frac{1}{2}}w^n_{1,i+\frac{1}{2}}\sqrt{g\,w^n_{1,i+\frac{1}{2}}}\frac{\rho_s-\rho_w}{2\rho^n_{i+\frac{1}{2}}} - \frac{1}{2}\frac{c^n_i-c^n_{i-1}}{\Delta x}c^n_{i-\frac{1}{2}}w^n_{1,i-\frac{1}{2}}\sqrt{g\,w^n_{1,i-\frac{1}{2}}}\frac{\rho_s-\rho_w}{2\rho^n_{i-\frac{1}{2}}}.$$

– Exner equation discretization,

$$z^{n+1}_i = z^n_i + \Delta t\frac{D^n_i}{1-p}$$

Let ς^{n+1}_i be the approximation of the free surface of water computed by the numerical scheme (41), therefore

$$\begin{aligned}\varsigma^{n+1}_i &= w^{n+1}_{1,i} + z^{n+1}_i \\ &= w^n_{1,i} - \frac{\Delta t}{2}\left(\frac{w^n_{1,i}-w^n_{1,i-1}}{\Delta x}\sqrt{g\,w^n_{1,i-\frac{1}{2}}} - \frac{w^n_{1,i+1}-w^n_{1,i}}{\Delta x}\sqrt{g\,w^n_{1,i+\frac{1}{2}}}\right) \\ &+ \frac{\Delta t}{2}\left(\frac{z^n_{i+1}-z^n_i}{\Delta x}\sqrt{g\,w^n_{1,i+\frac{1}{2}}} - \frac{z^n_i-z^n_{i-1}}{\Delta x}\sqrt{g\,w^n_{1,i-\frac{1}{2}}}\right) \\ &+ \delta\frac{\Delta t}{2}\left(\frac{c^n_{i+1}-c^n_i}{\Delta x}\,w^n_{1,i+\frac{1}{2}}\sqrt{g\,w^n_{1,i+\frac{1}{2}}}\frac{\rho_s-\rho_w}{2\rho^n_{i+\frac{1}{2}}}\right. \\ &\left. - \frac{c^n_i-c^n_{i-1}}{\Delta x}\,w^n_{1,i-\frac{1}{2}}\sqrt{g\,w^n_{1,i-\frac{1}{2}}}\frac{\rho_s-\rho_w}{2\rho^n_{i-\frac{1}{2}}}\right) - \Delta t\frac{D^n_i}{1-p} + z^n_i + \Delta t\frac{D^n_i}{1-p}.\end{aligned} \tag{78}$$

From (78) and taking into account that for this case $\delta = 0$, we get

$$\varsigma^{n+1}_i = \varsigma^n_i - \frac{\Delta t}{2}\left[\sqrt{g\,w^n_{1,i-\frac{1}{2}}}\left(\frac{\varsigma^n_i-\varsigma^n_{i-1}}{\Delta x}\right) - \sqrt{g w^n_{1,i+\frac{1}{2}}}\left(\frac{\varsigma^n_{i+1}-\varsigma^n_i}{\Delta x}\right)\right]. \tag{79}$$

Bearing in mind that at time $t = t_n$ the free surface is a constant function with respect of x, then we can conclude that $\varsigma^{n+1}_i = \varsigma^n_i$, which is mean that the free surface is a constant function.

The computed unit discharge by the numerical scheme (41) at time t_{n+1}, reads

$$\begin{aligned} w_{2,i}^{n+1} = \; & w_{2,i}^{n} - \frac{g\Delta t}{4\Delta x}\left((w_{1,i+1}^{n})^2 - (w_{1,i-1}^{n})^2\right) - \frac{g\Delta t}{2}\left(w_{1,i+\frac{1}{2}}\,\frac{z_{i+1}^{n} - z_{i}^{n}}{\Delta x}\right. \\ & \left. + \; w_{1,i-\frac{1}{2}}\,\frac{z_{i}^{n} - z_{i-1}^{n}}{\Delta x}\right) - \delta\frac{g\Delta t}{2}\left(\frac{c_{i+1}^{n} - c_{i}^{n}}{\Delta x} w_{1,i+\frac{1}{2}}^{2}\,\frac{\rho_s - \rho_w}{2\rho_{i+\frac{1}{2}}^{n}}\right. \\ & \left. + \; \frac{c_{i}^{n} - c_{i-1}^{n}}{\Delta x} w_{1,i-\frac{1}{2}}^{2}\,\frac{\rho_s - \rho_w}{2\rho_{i-\frac{1}{2}}^{n}}\right). \end{aligned} \tag{80}$$

Taking into account that $w_{1,i\pm\frac{1}{2}}$ is the arithmetic mean between the states, as well considering that $\delta = 0$, $z_i^n = \varsigma_i^n - w_{1,i}^n$ and $\varsigma_{n+1}^n = \varsigma_n^n$, the equation (80) reads

$$\begin{aligned} w_{2,i}^{n+1} = \; & w_{2,i}^{n} - \frac{g\Delta t}{4\Delta x}\left((w_{1,i+1}^{n})^2 - (w_{1,i-1}^{n})^2\right) \\ & - \frac{g\Delta t}{2}\left(\frac{w_{1,i}^{n} + w_{1,i+1}^{n}}{2}\,\frac{w_{1,i}^{n} - w_{1,i+1}^{n}}{\Delta x} \; + \frac{w_{1,i}^{n} + w_{1,i-1}^{n}}{2}\,\frac{w_{1,i-1}^{n} - w_{1,i}^{n}}{\Delta x}\right). \end{aligned} \tag{81}$$

Straightforward computations allow us conclude that $w_{2,i}^{n+1} = w_{2,i}^{n}$, which means that the numerical scheme compute null velocity on whole spatial domain.

The suspended sediment concentration computed by the numerical scheme (41) takes the form

$$\begin{aligned} w_{3,i}^{n+1} = \; & w_{3,i}^{n} - \frac{\Delta t}{2}\left(c_{i-\frac{1}{2}}^{n}\,\frac{w_{1,i}^{n} - w_{1,i-1}^{n}}{\Delta x}\sqrt{g\,w_{1,i-\frac{1}{2}}^{n}} - c_{i+\frac{1}{2}}\,\frac{w_{1,i+1}^{n} - w_{1,i}^{n}}{\Delta x}\sqrt{g\,w_{1,i+\frac{1}{2}}^{n}}\right) \\ & + \frac{\Delta t}{2}\left(c_{i+\frac{1}{2}}^{n}\sqrt{g\,w_{1,i+\frac{1}{2}}^{n}}\,\frac{z_{i+1}^{n} - z_{i}^{n}}{\Delta x} - c_{i-\frac{1}{2}}^{n}\sqrt{g\,w_{1,i-\frac{1}{2}}^{n}}\,\frac{z_{i}^{n} - z_{i-1}^{n}}{\Delta x}\right) \\ & + \delta\Delta t\left(\frac{c_{i+1}^{n} - c_{i}^{n}}{\Delta x} c_{i+\frac{1}{2}}^{n} w_{1,i+\frac{1}{2}}^{n}\sqrt{g\,w_{1,i+\frac{1}{2}}^{n}}\,\frac{\rho_s - \rho_w}{2\rho_{i+\frac{1}{2}}^{n}} - \frac{c_{i}^{n} - c_{i-1}^{n}}{\Delta x}\right. \\ & \left. c_{i-\frac{1}{2}}^{n} w_{1,i-\frac{1}{2}}^{n}\sqrt{g\,w_{1,i-\frac{1}{2}}^{n}}\,\frac{\rho_s - \rho_w}{2\rho_{i-\frac{1}{2}}^{n}}\right) - \Delta t D_i^n. \end{aligned} \tag{82}$$

Considering that under water at rest supposition $\delta = 0$, $z_i^n = \varsigma_i^n - w_{1,i}^n$ and $\varsigma_{n+1}^n = \varsigma_n^n$, equation (82) becomes in

$$\frac{w_{3,i}^{n+1} - w_{3,i}^{n}}{\Delta t} = -D_i^n. \tag{83}$$

From equations (79), (81) and (83) we can conclude the proof of proposition 1.

A similar proof can be done for the numerical scheme (59) which implements the non conservative form given by equation (28).

4.8 Wet-dry fronts

In shallow water flow simulations (e.g. floods, dam break, unsteady river flow) wet-dry fronts appears, where a wet region of the spatial domain becomes dry or vice versa. In these situations a boundary movement, defined by the wet-dry front, is produced. In order to obtain accurate, consistent results a suitable treatment is needed, [6].

On wet-dry fronts one or two conditions are imposed (see [12]). The first is the bed slope redefinition, which is made to obtain the exact balance between the wet-dry front and the pressure terms for the hydrostatic flux. If the bed slope is not redefined then spurious waves can appear. The second condition is of reflection.

In order to impose these conditions, a wet-dry parameter ε_{wd} is defined. Let us suppose that C_i and C_j are the wet cell and dry cell, respectively.

The balance condition (see [6]), is verified if

$$(\Delta z)_{i,j} = -\left((\Delta w_1)_{i,j} + (w_1)_{i,j}\left(\frac{\rho_s - \rho_w}{2\rho}\right)(\Delta c)_{i,j}\right). \tag{84}$$

On wet-dry fronts this condition is not verified, see Figure 6, and therefore the bed slope redefinition is needed, in order to do that, the rise of the bed is redefined as follows.

- Q-scheme of van Leer (41), Numerical scheme for non-conservative form (59).

$$\Delta z := \begin{cases} w_{1,i} - w_{1,j} + \dfrac{w_{1,i} + w_{1,j}}{2}\dfrac{\rho_s - \rho_w}{2\rho_{i,j}}(c_j - c_i) & \text{if} \quad w_{1,j} < \varepsilon_{wd} \quad \text{and} \\ & w_{1,i} - w_{1,j} < z_j - z_i, \\ z_j - z_i & \text{else.} \end{cases} \tag{85}$$

  Generally, the velocity in neighbouring cells of the wet-dry front is different from zero. In this situation the reflection condition imposes a unit averaged-flux discharge equal to zero at the wet-dry boundary.
- HLLCS Riemann solver. Since the accurate behaviour is obtained a similar way as the bed slope was approximated, (54), then a redefinition of rise of the bed is not needed.

Regarding the morphological changes, since the water depth appears in the denominator of the sediment entrainment formula, low water depth values might cause great erosion without physical sense, which can cause numerical instabilities, ([28]). The way to deal with this problem is the following:

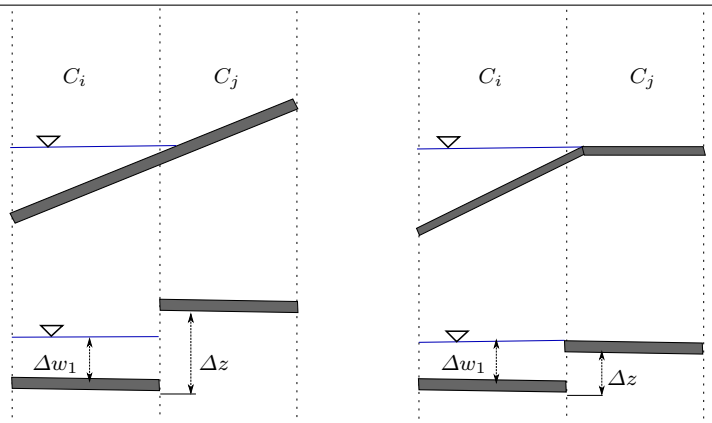

Fig. 6 Treatment of wet-dry fronts when both the scheme which implements the Q-scheme of van Leer and the non-conservative system are used.

- Q-scheme of van Leer and scheme of non-conservative form. A threshold value $\varepsilon_{_{ED}}$ is defined, so that, if the water depth in the cell C_j is less than $\varepsilon_{_{ED}}$, then the sediment entrainment is fixed at zero, [28].
- HLLCS Riemann solver. An interval of $(\mathcal{H}_0, \mathcal{H}_1)$ is established, to ensure that the volumetric sediment concentration always is analyzed in wet regions. If the water depth ranges from $\mathcal{H}_0$ to $\mathcal{H}_1$, then the values for sediment entrainment $E(x,t)$ and sediment deposition $D(x,t)$ are fixed at zero. However if the water depth is less than $\mathcal{H}_0$, then the unit discharge is also fixed at zero, see Figure 7. This interval improves the numerical stability, but it can induce a reduction of the zones where the wet-dry front and the bed evolution are approximated. In [19] is proposed that only values of the characteristic speeds of wet cells are taken into account. This criteria is written as follows.

$$\lambda_i = \begin{cases} u_i - \sqrt{\dfrac{g w_{1,i}}{2}} & \text{if} \quad w_{1,j} < \mathcal{H}_1, \\ \lambda_i & \text{else.} \end{cases} \tag{86}$$

$$\lambda_{i+1} = \begin{cases} u_i + 2\sqrt{\dfrac{g w_{1,i}}{2}} & \text{if} \quad w_{1,j} < \mathcal{H}_1, \\ \lambda_{i+1} & \text{else.} \end{cases} \tag{87}$$

5 Numerical Results

In order to measure the accuracy of the numerical schemes described earlier, several numerical experiments were carried out. In the first test, the steady stationary solution conditions are recreated. In the second test, a dam break, when the whole spatial domain is wet, is reproduced. Finally, three experimental dam breaks were reproduced and the numerical results were compared with the experimental data.

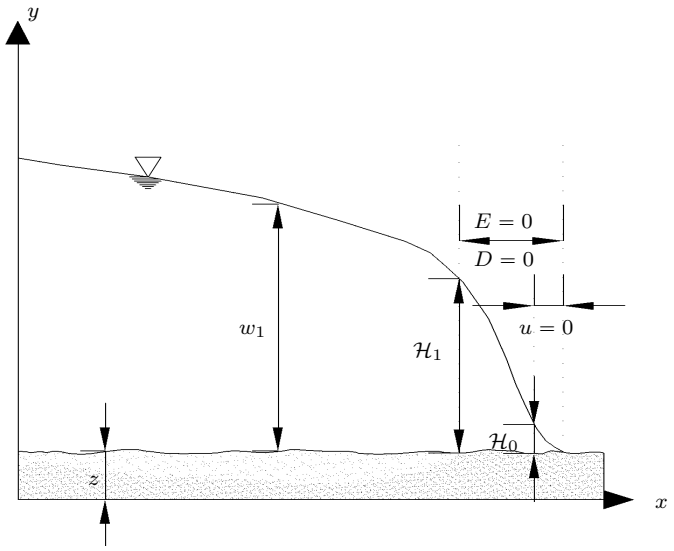

Fig. 7 Interval to treat the bed evolution close of wetting drying fronts when the HLLCS approximate Riemann solver is used.

5.1 Parameters for the both mathematical model and the numerical model, initial conditions and boundary conditions

The values for the physical parameters are shown in Table 2, while the values for the numerical parameters, for each numerical scheme, are displayed in Tables 3 and 4. The values for the dimensionless parameters are shown in Table 5. The spatial domain for each numerical experiment can be seen in Table 6, and the initial conditions are displayed in Table 7. Finally, in Table 8, the imposed boundary conditions are given. The numerical experiments mentioned in these tables are as follows:

- Experiment 1. Compute of steady stationary solution.
- Experiment 2. Simulation of a dam break, described in [8].
- Experiment 3. Simulation of an experimental dam break carried out in the Universitè Catholique of Louvain, and shown in [41].
- Experiments 4 and 5. Numerical simulation of conditions for a small-scale laboratory dam break, as in [37].

Remark 1 *The numerical scheme, where the source terms* $\mathbf{S}_1$ *and* $\mathbf{S}_4$ *are discretised in upwind form, is denoted by QSVLUS1S4, while the numerical scheme which implements the non-conservative system is denoted by QSVL-NCP.*

Table 2 Physical parameters for numerical experiments.

Experiment	ρ_s (kg/m^3)	ρ_w (kg/m^3)	s (kg/m^3)	d (mm)	ν (m^2/s)
Experiment 1	2650	1000	1650	4	1.2×10^{-6}
Experiment 2	2650	1000	1650	4	1.2×10^{-6}
Experiment 3	1540	1000	1540	3.5	1.2×10^{-6}
Experiment 4	2580	1000	1580	3.9	1.2×10^{-6}
Experiment 5	2580	1000	1580	3.9	1.2×10^{-6}

Table 3 Numerical parameters for QSVLUS1S4 and QSVLNCP, $\widehat{t}_0 = \sqrt{h_l/g}$.

Parameters	CFL	ε_{HR}	ε_{WD}	ε_{ED}	T_f (s)	Nodes	A_g
Experiment 1	0.5	0.0001	0.0001	0.0012	60	300	0.01
Experiment 2	0.7	10	0.001	0.001	120	1000	0
Experiment 3	0.3	3	0.005	0.001	$10\ \widehat{t}_0$	300	0.008
Experiment 4	0.35	5	0.003	0.01	1.25	600	0.0025
Experiment 5	0.35	5	0.008	0.01	1.25	600	0.0065

Table 4 Numerical parameters for HLLCS approximate Riemann solver, $\widehat{t}_0 = \sqrt{h_l/g}$.

Parameters	CFL	$(\mathcal{H}_0, \mathcal{H}_1)$	T_f (s)	Nodes	A_g
Experiment 1	0.4	$(0.01, 0.012)$	60	5000	0.01
Experiment 2	0.4	$(0, 0.001)$	120	1000	0
Experiment 3	0.4	$(0.05, 0.07)$	$10\widehat{t}_0$	150	0.0011
Experiment 4	0.4	$(0, 0.001)$	1.25	600	0.0011
Experiment 5	0.4	$(0, 0.001)$	1.25	400	0.005

Table 5 Dimensionless values used in numerical experiments.

Parameters	η		θ_c		ϕ		p	
	QS	HLLCS	QS	HLLCS	QS	HLLCS	QS	HLLCS
Experiment 1	0.02	0.02	0.045	0.045	10	10	0.4	0.4
Experiment 2	0.03	0.02	0.045	0.045	10	10	0.4	0.4
Experiment 3	0.03	0.02	0.045	0.045	4	0.4	0.4	0.4
Experiment 4	0.0165	0.009	0.047	0.047	2	0.5	0.47	0.47
Experiment 5	0.0165	0.009	0.047	0.047	1	0.2	0.47	0.47

5.2 Experiment 1

In Figures 8-11, we can see the numerical results given by three numerical schemes. Figure 8 shows the comparison between the initial free surface and the final compute free surface, from this figure we can see no one variations of the final free surface with respect of the initial free surface. This fact is confirmed in Figure 9, where the error for compute free surface is shown. Notice

Table 6 Spatial domain for numerical experiments.

Experiment	Exp. 1	Exp. 2	Exp. 3	Exp. 4	Exp. 5
Domain	$[-5, 10]$	$[20000, 30000]$	$[0, 2.5]$	$[-3, 3]$	$[-3, 3]$

Table 7 Initial conditions for the numerical experiments. Here $\Omega_d = [\frac{3\pi}{2} - 6, \frac{7\pi}{2} - 6]$ and Ω_w is the complement of Ω_d.

Experiment	$z(x, t_0)$	$w_1(x, t_0)$	$u(x, t_0)$	$c(x, t_0)$
Experiment 1	$\sin(x + 6) + 1$ if $x \in \Omega_d$ 0 if $x \in \Omega_w$	$1.5 - z(x, t_0)$ if $x \in \Omega_w$ 0 if $x \in \Omega_d$	0	0.3 $x \in \Omega_w$ 0 if $x \in \Omega_d$
Experiment 2	0	40 if $x \in [20000, 25000]$ 2 if $x \in [25000, 30000]$	0	0
Experiment 3	0	0.1 if $x \in [0, 1.25]$ 0 if $x \in [1.25, 2.5]$	0	0
Experiment 4	0	0.35 if $x \in [-3, 0]$ 0 if $x \in [0, 3]$	0	0
Experiment 5	0.1 if $x \in [-3, 0]$ 0 if $x \in [0, 3]$	0.25 if $x \in [-3, 0]$ 0.1 if $x \in [0, 3]$	0	0

Table 8 Boundary conditions.

	Left end	Right end
Experiment 1	Wall	Wall
Experiment 2	Inflow	Outflow
Experiment 3	Inflow	Outflow
Experiment 4	Inflow	Outflow
Experiment 5	Inflow	Outflow

that the errors of the three numerical schemes are in the order of machine epsilon. As well, in Figure 8 it is observed that the depth of the bottom increases as effect of the sediment deposition, as it was expected. Figure 10 shows that the three numerical scheme compute null velocity over whole domain, because the compute velocities are in the order of machine epsilon. From equation (73) we have that the volumetric sediment concentration decreases as a function of time, if $c(x, t) < 1 - p$. This fact is well recreate by our numerical scheme, as it is depicted in Figure 11, where the absolute value of the difference between the left hand site and the right hand site of (73) can be seen. Notice that the numerical scheme are computing a difference in the order of 1×10^{-15}. Therefore we can conclude that the numerical schemes presented in this work compute correctly the steady solution, which is mean that our numerical schemes are well balanced.

5.3 Experiment 2

The dam break conditions shown in [8] were simulated in this numerical test. Both the water free surface and the depth of bed at $t = 20\,\mathrm{s}$ are shown in Figure 12. Note that the water free surface computed by the three numerical schemes is an accurate approximation of the results shown in [8]. Regarding the numerical results of the depth of bed, it can be seem that the HLLCS scheme estimates more sediment entrainment where the dam break was centered, while the schemes QSVLUS1S4 and QSVLNCP accurately approximate the morphological changes.

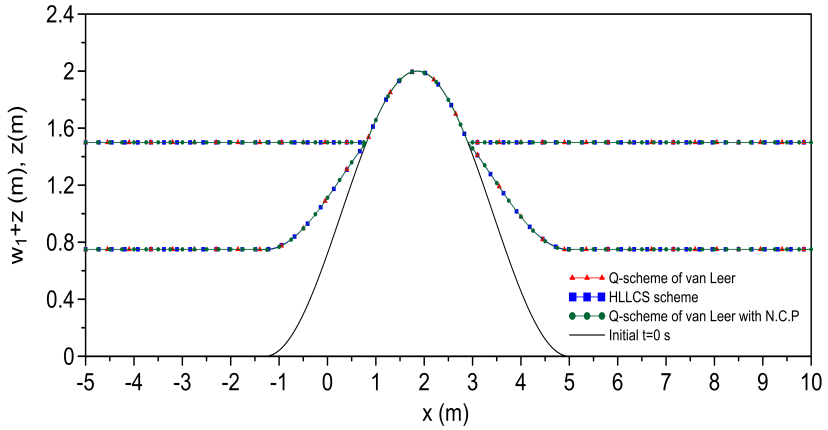

Fig. 8 Free surface of water and depth of bed at $t = 60\,\mathrm{s}$.

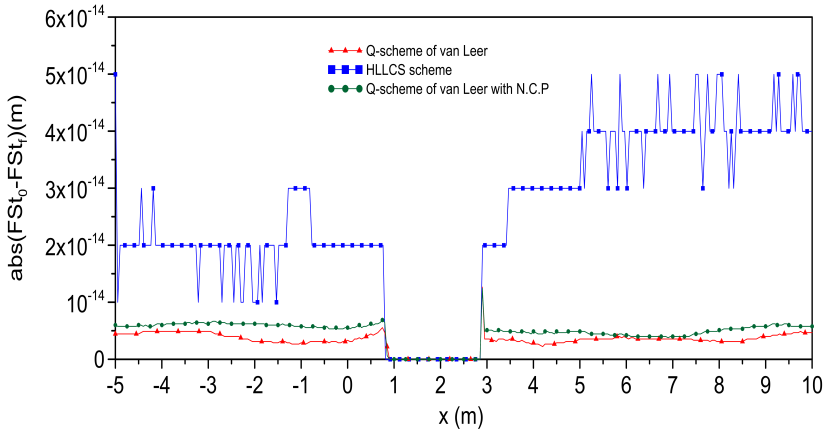

Fig. 9 Error in the compute of the free surface of water at $t = 60s$.

Figures 13 and 14 show the results obtained for the velocity at $t = 20\,\mathrm{s}$ and $t = 120\,\mathrm{s}$, respectively. The results provided by the three numerical schemes at $t = 20\,\mathrm{s}$ are very similar to the results of Cao. However, for $t = 120\,\mathrm{s}$ in the region where the water front is computed, the computed velocity is less than the of [8], but the approximation is correct.

Both the expansion wave and shock wave shown by Cao are recreated exactly by the three numerical schemes. Likewise, the velocity and morphological changes are estimated correctly. Thus, the three numerical schemes reproduce accurately the numerical results of [8].

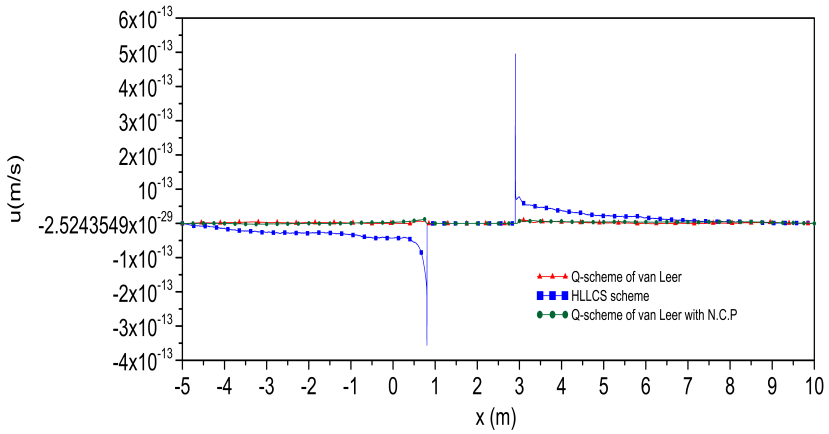

Fig. 10 Velocity at $t = 60\,\mathrm{s}$.

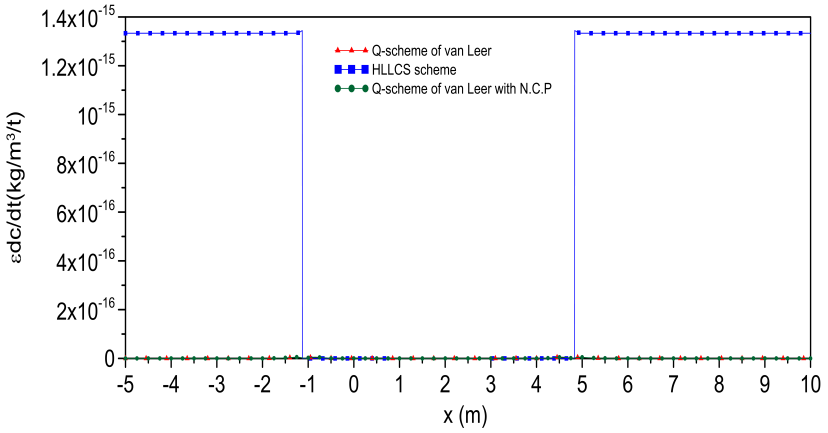

Fig. 11 Error for the compute of temporal evolution of volumetric sediment concentration at $t = 60\,\mathrm{s}$.

5.4 Experiment 3

In order to measure the accuracy of our numerical schemes, the experimental dam break flows carried out in Louvain-la-Neuve (Universitè Catholique de Louvain [20]) were numerically simulated and the results obtained were compared with the experimental data.

Figures 15 – 17 show the numerical results of the three numerical schemes against the experimental data. The downstream free surface of water computed by schemes QSVLS1S4 and QSVLNCP is greater than the water free surface given for the experimental data in this region. However the approximation is sufficient. Moreover, the results provided by HLLCS scheme are an

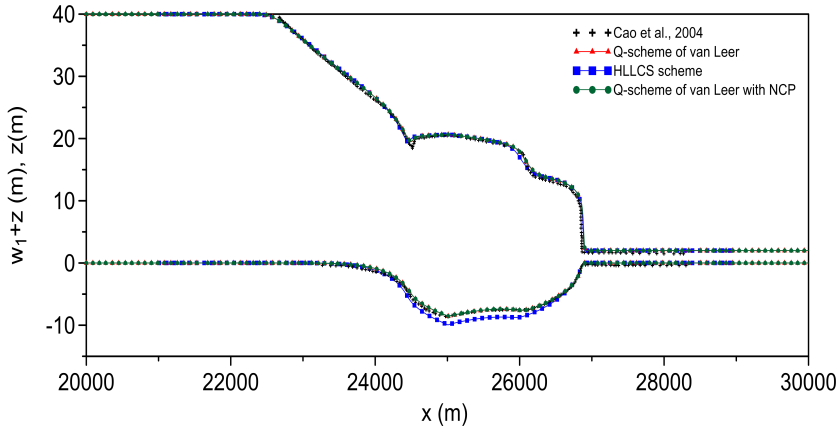

Fig. 12 Water free surface and bed the depth computed at $t = 120\,\mathrm{s}$.

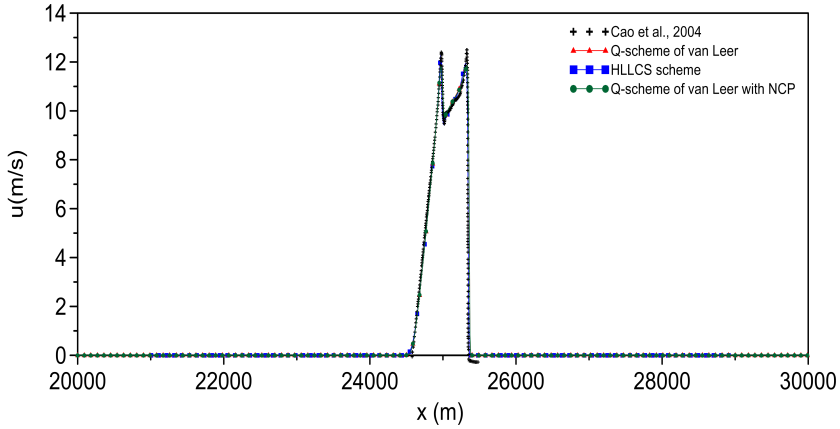

Fig. 13 Velocity computed at $t = 20\,\mathrm{s}$.

accurate approximation for the downstream water free surface. It should be noted that the up-stream numerical water free surface obtained is less than the experimental data of the water free surface in this region, but the differences are minor. The hydraulic jump observed in the experimental data is better approximated by the HLLCS scheme. Regarding the water front advance, it can be seen that the three numerical schemes are accurate.

Regarding the bed evolution, Figures 15 and 16, show that the up-stream morphological evolution computed by the HLLCS scheme, at times $5\,\widehat{t}_0$ and $7.5\,\widehat{t}_0$, are less than the morphological changes observed in the experimental data. On the other hand, the upstream morphological evolution computed by both schemes QSVLS1S4 and QSVLNCP is in accordance with the experimental data. Furthermore at time 10 $\widehat{t}_0$ both schemes QSVLS1S4 and QSVLNCP

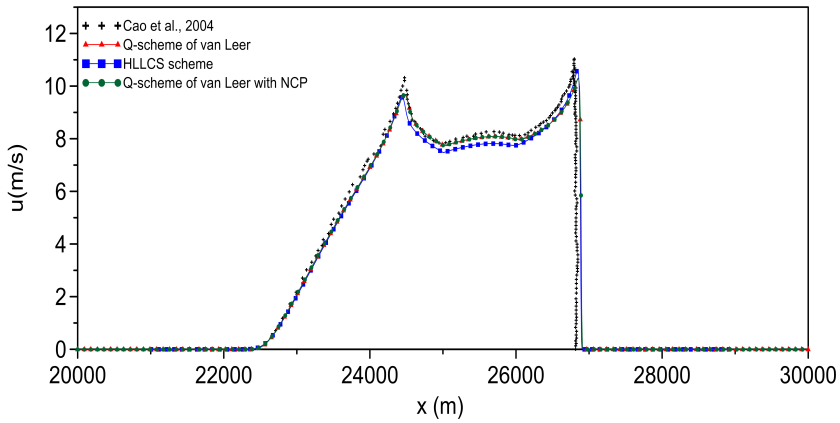

Fig. 14 Velocity computed at $t = 120\,\mathrm{s}$.

compute more upstream sediment entrainment than that observed one in the experimental data, while the upstream sediment entrainment computed by the HLLCS scheme fit better to the experimental data. The downstream sediment entrainment computed by the three numerical schemes is greater than the experimental data for every computed time, although the computed approximation is good enough.

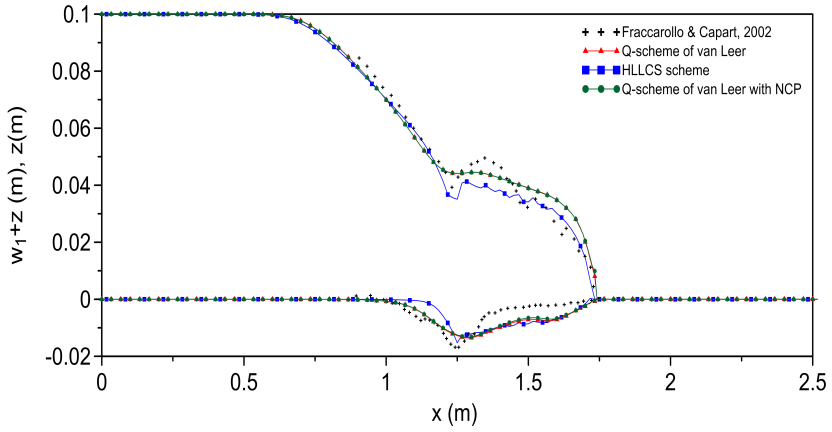

Fig. 15 Water free surface and the bed depth computed at $5\,\widehat{t}_0$.

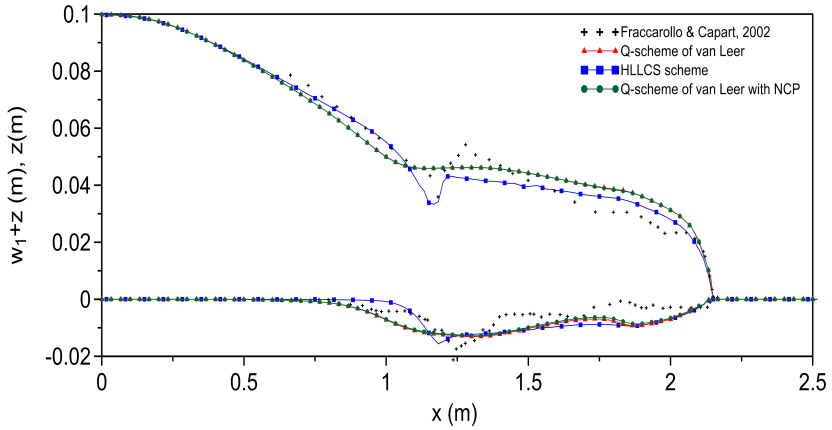

Fig. 16 Water free surface and the bed depth computed at $7.5\,\widehat{t}_0$.

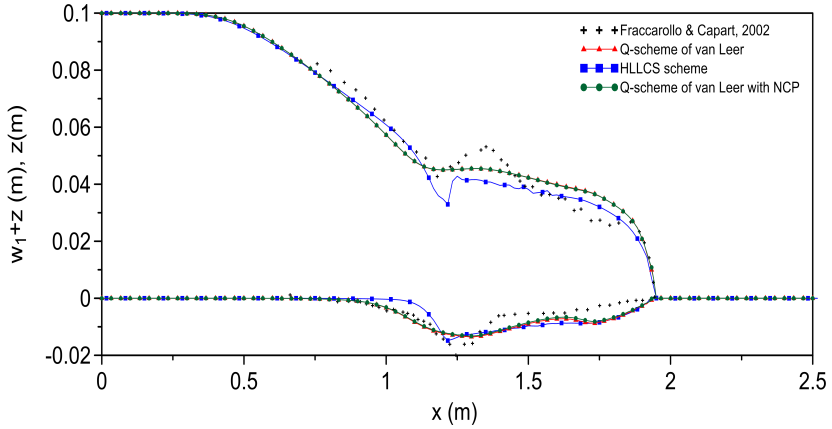

Fig. 17 Water free surface and the bed depth computed at $10\,\widehat{t}_0$.

5.5 Experiments 4 and 5

In these numerical experiments the conditions of small scale dam breaks, performed in the Universitè Catholique of Louvain, were recreated. Both the values for physical parameter and the experimental data were obtained from [37].

The results computed in the fourth numerical experiment are shown in Figure 18.

It can be seen that the downstream sediment entrainment computed by the HLLCS scheme is greater than the downstream sediment entrainment provided by the experimental data. However, the differences between them are small. The upstream sediment entrainment computed by the HLLCS scheme is in

accordance with the experimental data. The bed evolution computed by both schemes QSVLS1S4 and QSVLNCP reproduce accurately the bed changes.

From Figure 18 it can be seen that the region where the hydraulic jump took place is correct for the three numerical schemes, but the experimental water free surface is not given correctly by the numerical results.

The downstream conditions for the water free surface are correctly reproduced by the numerical schemes because the numerical results and experimental data have the same qualitative form. Notice that the downstream free surface of water computed by both schemes QSVLS1S4 and QSVLNCP is greater than the experimental water free surface although the adjustment made is adequate. Moreover, the water free surface computed by the HLLCS scheme fits accurately the experimental water free surface.

Regarding the water front advance, it can be seen that the results obtained by the HLLCS scheme are faster than the experimental data while the results provided by the other two methods calculated more accurately.

The numerical results of the fifth numerical experiment are shown in Figure 19. We can see that the hydraulic jump is only partially reproduced by the three numerical schemes; there is a gap between the place provided by the experimental data and that calculated by the numerical schemes. The computed water free surface after the hydraulic jump is in good agreement with the experimental data. Notice that the water front advance computed by the three numerical schemes presents a gap in comparison with the water front advance observed in the experimental data. Regarding the morphological changes, the tendency observed in the experimental data is correctly represented by the three numerical schemes. The HLLCS scheme produces more upstream sediment entrainment than that observed one in the experimental data, but the differences are minor. The adjustment of the upstream bed evolution made by the schemes QSVLS1S4 and QSVLNCP is satisfactory. The downstream bed evolution computed by the three numerical schemes is in good agreement with the experimental bed evolution. In these numerical tests small oscillations, are noticeable where the hydraulic jump took place, produced by the HLLCS schemes while the results of QSVLS1S4 and QSVLNCP gives a smooth tendency.

6 Conclusions

Three numerical schemes to simulate dam break flows with suspended load and bedload sediment transport have been presented. Two of them implement the Q-scheme of van Leer to compute the numerical flux and the other one implements a HLLC Riemann solver. In one of the presented numerical scheme, the source terms related to the bed slope and the sediment concentration variations are discretised in an upwind way. In a second numerical scheme, the bed slope source term is discretised in an upwind way but the source term related to the variation of sediment concentration is treated as a non

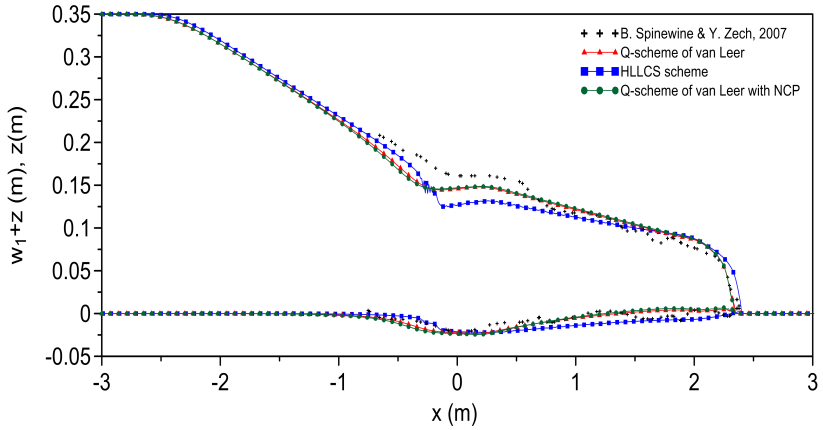

Fig. 18 Free surface of water and bed depth computed at $t = 1.25\,\mathrm{s}$.

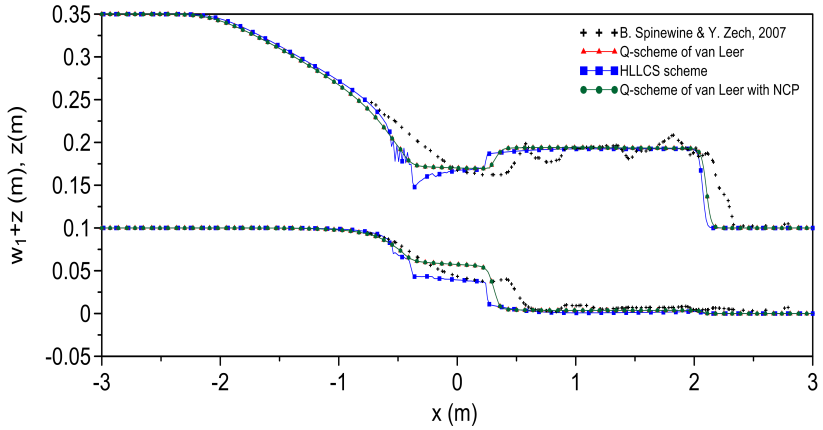

Fig. 19 Free surface of water and bed depth computed at $t = 1.25\,\mathrm{s}$.

conservative product. The last one numerical scheme, the HLLCS Riemann solver, take into account the bed slope source term inside of the numerical flux whiles the sediment concentration variation is computed in a explicit way.

We have proved that the numerical schemes are well-balanced, by the numerical results of the steady stationary solution test. The contrast made between the numerical results and the experimental data shows that the numerical schemes accurately compute the water front advance. It can be seen that the computed free surface of water recreates in successfully the free surface of water of the experimental data. Regarding to bed evolution, we have seen that the three numerical scheme compute a successful approximation for the observed bed evolution in the experimental data. Due to that the Grass parameter is close to zero, the interaction between the flux and the bottom is

weak for the physical experiments simulated in this work. From the different numerical tests carried out, we can conclude that the computed water front advance depends on the wet-dry parameter ε_{WD}, the threshold value for sediment entrainment ε_{ED} or the interval $(\mathcal{H}_0, \mathcal{H}_1)$. We have also seen that the constant value ϕ, in the sediment entrainment formula, helps to improve the computation of the water front advance. Therefore an interesting future work is try to developed an uncertainty quantification study about these parameters.

Acknowledgements

The authors are grateful to the Consejo Nacional de Ciencia y Tecnología for the scholarship granted to carry out this project. This work was partially supported by the Spanish MICINN project MTM2013-43745-R and MTM2017-86459-R and by the Xunta de Galicia, the FEDER under research project ED431C 2017/60 -014 and was partially supported by PRODEP project UAM-PTC-669.

References

1. D. D. Apsley and P. K Stansby. Bed-load sediment transport on large slopes: model formulation and implementation within a RANS solver. *J. Hydraul. Eng.*, 134(10):1440–1451, 2008.
2. Faranak Behzadi and James C Newman III. An exact source-term balancing scheme on the finite element solution of shallow water equations. *Comput. Methods. Appl. Mech. Eng.*, 359:112662, 2020.
3. F. Benkhaldoun, S. Sari, and M Seaid. A flux-limiter method for dam-break flows over erodible sediment beds. *Applied Mathematical Modelling*, 36(10):4847 – 4861, 2012.
4. A. Bermúdez, X. López, and M. E Vázquez-Cendón. Numerical solution of non-isothermal non-adiabatic flow of real gases in pipelines. *J. Comput. Phys.*, 323:126 – 148, 2016.
5. A. Bermúdez and M. E Vázquez-Cendón. Upwind methods for hyperbolic conservation laws with source term. *Comput. Fluids*, 23(8):1049–1071, 1994.
6. P. Brufau, P. García Navarro, and M. E Váquez-Cendón. Zero mass error using unsteady wetting-drying conditions in shallow water flows over dry irregular topography. *Int. J. Numer. Methods Fluids*, 45(10):1047–1082, 2004.
7. F. N. Cantero-Chinchilla, O. Castro-Orgaz, S. Dey, and J. L Ayuso-Muñoz. Nonhydrostatic dam break flows. II: one-dimensional depth-averaged modeling for movable bed flows. *J. Hydraul. Eng.*, 142(12):04016069, 2016.
8. Z. Cao, G. Pender, S. Wallis, and P Carlling. Computational dam-break hydraulics over erodible sediment bed. *J. Hydraul. Eng.*, 130(7):689–703, 2004.
9. H. Capart and D Young. Formation a jump by the dam-break wave over a granular bed. *J. Fluid Mech.*, 372:165–187, 1998.
10. M. J. Castro-Díaz, E. D. Fernández-Nieto, and A. M Ferreiro. Sediment transport models in shallow water equations and numerical approach by high order finite volume methods. *Comput. Fluids*, 37(3):299 – 316, 2008.
11. M. J. Castro-Díaz, E. D. Fernández-Nieto, T. Morales de Luna, G. Narbona-Reina, and C Parés. A HLLC scheme for nonconservative hyperbolic problems. application to turbidity currents with sediment transport. *Esaim Math. Model Numer. Anal.*, 47:1–32, 2013.
12. L Cea. *An unstructured finite volume model for unsteady turbulent shallow water flow with wet-dry fronts: numerical solver and experimental validation.* PhD thesis, Universidade da Coruña, 2005.

13. S. Cordier, M.H. Le, and T Morales de Luna. Bedload transport in shallow water models: Why splitting (may) fail, how hyperbolicity (can) help. *Adv. Water. Resour.*, 34(8):980 – 989, 2011.
14. H. A Einstein. The bed load function for sediment transportation in open channel flows. Bulletin 1026, Department of Agriculture, Soil Conservation Service, Washington, D.C., 1950.
15. Fateme Ebrahimi Erami and Ali Rahmani Firoozjaee. Numerical solution of bed load transport equations using discrete least squares meshless (dlsm) method. *Applied Mathematical Modelling*, 77:1095–1109, 2020.
16. F. M Exner. Zur physik der dünen. *Akad. Wiss. Wien Math. Naturwiss, Klasse*, 129:929–952, 1920.
17. F. M Exner. Über die wechselwirkung zwischen wasser und geschiebe in flüsen. *Akad. Wiss. Wien Math. Naturwiss, Klasse*, 134:165–2014, 1925.
18. Ali Rahmani Firoozjaee and Mostafa Sahebdel. Element-free galerkin method for numerical simulation of sediment transport equations on regular and irregular distribution of nodes. *Eng. Anal. Bound. Elem.*, 84:108–116, 2017.
19. L. Fraccarollo and E. F Toro. Experimental and numerical assessment of the shallow water model for two-dimensional dam-break type problems. *J. Hydraul. Res.*, 33(6):843–864, 1995.
20. L. Fraccarrollo and H Capart. Riemann wave description of erosional dam-break flows. *J. Fluid Mech.*, 461:183–238, 2002.
21. A. J Grass. Sediment transport by waves and currents. Technical Report FL29, SERC. London Cent. Mar, 1981.
22. A Harten. On class of high resolution total-variation-stable finite-difference schemes. *SIAM J. Numer. Anal.*, 21(1):1–23, 1984.
23. P. Hu and Z Cao. Fully coupled mathematical modeling of turbidity currents over erodible bed. *Adv. Water. Resour.*, 32(1):1 – 15, 2009.
24. C. Juez, J. Murillo, and P García-Navarro. A 2D weakly-coupled and efficient numerical model for transient shallow flow and movable bed. *Adv. Water. Resour.*, 71:93 – 109, 2014.
25. R. J LeVeque. *Finite-Volume methods for hyperbolic problems*. Cambridge University Press., 2002.
26. J. Li, Z. Cao, G. Pender, and L Qingquan. A double layer-averaged model for dam-break flows over mobile bed. *J. Hydraul. Res.*, 51(5):518–534, 2013.
27. S. Li and C. J Duffy. Fully coupled approach to modeling shallow water flow, sediment transport, and bed evolution in rivers. *Water Resour. Res.*, 47(3):W03508, 2011.
28. X. Liu, J. A. Infante Sedano, and A Mohammadian. A robust coupled 2-D model for rapidly varying flows over erodible bed using central-upwind method with wetting and drying. *Can. J. Civ. Eng.*, 42(8):530–543, 2015.
29. X. Liu, A. Mohammadian, A. Kurganov, and J. A Infante Sedano. Well-balanced central-upwind scheme for a fully coupled shallow water system modeling flows over erodible bed. *J. Comput. Phys.*, 300:202 – 218, 2015.
30. E. Meyer-Peter and R Müller. Formulas for bed-load transport. Technical report, 2nd Meet. Int. Assoc. Hydraul. Struct. Res., Stockholm, 1948. 39-64.
31. J. Murillo and P García-Navarro. An exner-based coupled model for two-dimensional transient flow over erodible bed. *J. Comput. Phys.*, 229(23):8704 – 8732, 2010.
32. J. Murillo and P García-Navarro. Augmented versions of the HLL and HLLC riemann solvers including source terms in one and two dimensions for shallow flow applications. *J. Comput. Phys.*, 231(20):6861–6906, 2012.
33. Khawar Rehman and Yong-Sik Cho. A novel well-balanced scheme for spatial and temporal bed evolution in rapidly varying flow. *J. Hydro-environ. Res.*, 27:87–101, 2019.
34. P. L Roe. A basis for upwind differencing of the two-dimensional unsteady Euler equations. *Numerical Methods for Fluid Dynamics II*, pages 55–80, 1986.
35. A Shields. *Anwendung der Aehnlichkeitsmechanik und der Turbulenzforschung auf die Geschiebebewegung*. PhD thesis, University Berlin, 1936.
36. S. Soares-Frazão and Y Zech. HLLC scheme with novel wave-speed estimators appropriate for two-dimensional shallow-water flow on erodible bed. *Int. J. Numer. Methods Fluids*, 66(9):1019–1036, 2011.

37. B. Spinewine and Y Zech. Small-scale laboratory dam-break waves on movable beds. *J. Hydraul. Res.*, 45(sup1):73–86, 2007.
38. E. F Toro. *Shock-capturing methosd for free-surface shallow flows*. Wiley & Sons, Ltd, 2001.
39. E. F. Toro, M. Spruce, and W Speares. Restoration of the contact surface in the HLL-Riemann solver. *Shock waves*, 4(1):25–34, 1994.
40. L. C Van Rijn. Sediment transport, part I: Bed load transport. *J. Hydraul. Eng.*, 110(10):1431–1456, 1984.
41. W. Wu and S. S Wang. One-dimensional modeling of dam-break flow over movable beds. *J. Hydraul. Eng.*, 133(1):48–58, 2007.
42. R. Zhang and J Xie. *Sedimentation research in China: Systematic selection*. China and Water and Power Press, Beijing, 1993.